MUCOSAL IMMUNITY

Unresponsiveness to inhaled antigen is governed by conventional dendritic cells and overridden during infection by monocytes

James G. Bedford[1], Melanie Heinlein[2,3], Alexandra L. Garnham[2,3], Thi H. O. Nguyen[1], Tom Loudovaris[4], Chenghao Ge[1,5], Stuart I. Mannering[4], Michael Elliott[6,7], Stuart G. Tangye[8,9], Katherine Kedzierska[1], Daniel H. D. Gray[2,3], William R. Heath[1], Linda M. Wakim[1]*

The nasal-associated lymphoid tissues (NALTs) are mucosal-associated lymphoid organs embedded in the submucosa of the nasal passage. NALTs represent a known site for the deposition of inhaled antigens, but little is known of the mechanisms involved in the induction of immunity within this lymphoid tissue. We find that during the steady state, conventional dendritic cells (cDCs) within the NALTs suppress T cell responses. These cDCs, which are also prevalent within human NALTs (tonsils/adenoids), express a unique transcriptional profile and inhibit T cell proliferation via contact-independent mechanisms that can be diminished by blocking the actions of reactive oxygen species and prostaglandin E_2. Although the prevention of unrestrained immune activation to inhaled antigens appears to be the default function of NALT cDCs, inflammation after localized virus infection recruited monocyte-derived DCs (moDCs) to this region, which diluted out the suppressive DC pool, and permitted local T cell priming. Accommodating for inflammation-induced temporal changes in NALT DC composition and function, we developed an intranasal vaccine delivery system that coupled the recruitment of moDCs with the sustained release of antigen into the NALTs, and we were able to substantially improve T cell responses after intranasal immunization. Thus, homeostasis and immunity to inhaled antigens is tuned by inflammatory signals that regulate the balance between conventional and moDC populations within the NALTs.

INTRODUCTION

Lymphoid organs have evolved to service the upper respiratory tract (URT) and facilitate the induction of immune responses to inhaled antigens and include encapsulated draining lymph nodes (LNs) and mucosal-associated lymphoid tissue, which are directly embedded in the submucosa of the nasal passage. In humans, the adenoids, the palatine tonsils, and the bilateral lingual tonsils form a ring of mucosal-associated lymphoid tissue situated at the upper end of the pharynx collectively known as Waldeyer's ring. The murine equivalent, the nasal-associated lymphoid tissue (NALT), consists of paired lymphoid tissue located on the floor of the nasal cavity near the entrance of the nasopharyngeal duct. NALTs are highly organized lymphoid structures that feature high endothelial venules (HEVs) and T cell– and B cell–enriched areas that develop postnatally (*1*), independent of several factors known to be involved in the organogenesis of LNs and other mucosal embedded lymphoid tissue (i.e., Peyer's patches) (*2*). NALTs are strategically located to orchestrate regional immune responses and are a recognized site for the deposition of inhaled antigens. However, little is known of the immunity that can be evoked within this lymphoid tissue or of the mechanisms that drive immune responses to airborne pathogens and intranasal vaccines, yet concurrently enforce tolerogenic responses to commensal organisms and harmless inhaled environmental irritants that are also routinely encountered within this lymphoid tissue.

Here, we examined the contribution of dendritic cells (DCs) present in the NALTs in the generation of cellular immunity to inhaled antigens. We find that during the steady state, DCs within the NALTs fail to prime T cell responses and, instead, actively block T cell activation via a contact-independent mechanism that can be diminished by blocking the actions of reactive oxygen species (ROS) and prostaglandin E_2 (PGE_2). Whereas the prevention of unwarranted immune activation to inhaled antigens appears the default function of DCs in the NALTs, local inflammation induced by infection, but not exposure to commensal bacteria, resulted in the influx of monocyte-derived DCs (moDCs), which transformed this lymphoid tissue into an environment that can support the initiation of cellular immune responses. These data indicate that the balance between immunity and homeostasis to inhaled antigens is orchestrated by NALT DCs.

RESULTS

DCs in the NALTs fail to activate T cell responses

NALTs, identified by microscopy of nasal tissue sections as aggregates of organized lymphoid tissue found on both sides of the nasopharyngeal duct, dorsal to the soft palate (*3*) are highly organized lymphoid structures that feature HEV as well as T cell– and B cell–enriched areas (Fig. 1, A to C). We investigated the mechanism and kinetics of antigen presentation after antigen delivery into the upper airways. DC subsets present within the NALTs were compared with matched subsets present within the cervical LNs (cLNs), the encapsulated LNs that drain the URT. In the NALTs, conventional

[1]Department of Microbiology and Immunology, University of Melbourne, Peter Doherty Institute for Infection and Immunity, Melbourne, Victoria 3000, Australia. [2]Walter and Eliza Hall Institute of Medical Research, Melbourne, Victoria, Australia. [3]Department of Medical Biology, University of Melbourne, Melbourne, Victoria, Australia. [4]Immunology and Diabetes Unit, St Vincent's Institute of Medical Research, Fitzroy, Victoria 3065, Australia. [5]School of Medicine, Tsinghua University, Beijing, China. [6]Sydney Medical School, University of Sydney, Sydney, New South Wales 2006, Australia. [7]Chris O'Brien Lifehouse Cancer Centre, Royal Prince Alfred Hospital, Camperdown, New South Wales 2050, Australia. [8]Immunity & Inflammation Theme, Garvan Institute of Medical Research, Darlinghurst, New South Wales 2010, Australia. [9]St Vincent's Clinical School, University of New South Wales, Sydney, New South Wales 2052, Australia.
*Corresponding author. Email: wakiml@unimelb.edu.au

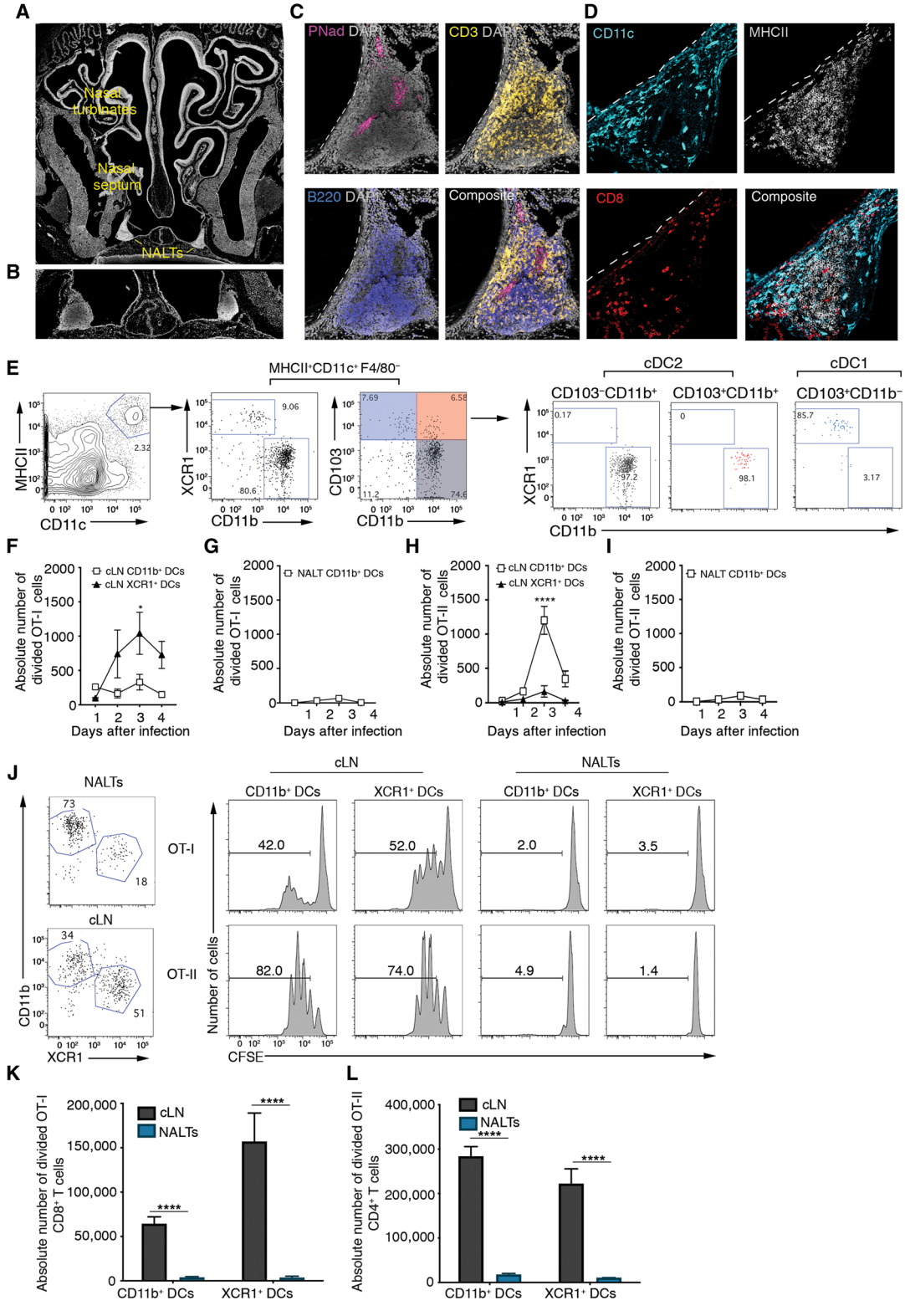

Fig. 1. DCs in the NALTs fail to present viral and cell-associated antigen. (**A** and **B**) Microscopy of the nasal tissue highlighting the NALTs, nasal turbinates, and nasal septum. (**C**) Microscopy of the NALTs with the B220 (B cell zone), CD3 (T cell zone), peripheral node addressin (PNad), and 4′,6-diamidino-2-phenylindole (DAPI) staining. Dotted lines indicate epithelial layer. (**D**) Immunohistochemistry on the NALTs of mice staining for CD11c (blue), CD8 (red), and MHCII (gray). (**E**) Representative flow cytometry profiles gated on MHCII$^+$CD11c$^+$F4/80$^-$ cells from the NALTs depicting the expression of CD11b$^+$ and XCR1$^+$ on the CD103$^+$CD11b$^+$ (red), CD103$^-$CD11b$^+$(gray), and CD103$^+$CD11b$^-$ (blue) DC subsets. (**F** to **I**) Proliferation of CFSE-labeled (F and G) OT-I or (H and I) OT-II cells cultured for 60 hours together with DC subsets [identified as in (E)] isolated from (F and H) cLN or (G and I) NALTs of mice infected intranasally 1 to 4 days earlier with x31-OVA$_1$ or x31-OVA$_2$. Data are pooled from three to eight experiments per time point. Symbols represent means ± SEM (two-way ANOVA, Sidak's multiple comparison). (**J** to **L**) Proliferation of CFSE-labeled OT-I or OT-II cells cultured for 60 hours together with OVA-coated H2-K^{bm1}splenocytes (OCS) and DC subsets (identified as depicted in the fluorescence-activated cell sorting profiles) isolated from cLN or NALTs of mice injected subcutaneously with B16-Flt3-L tumor 10 days earlier. (J) Representative histograms of CFSE dilution of OT-I and OT-II cells after 60-hour culture. The absolute number of divided (K) OT-I and (L) OT-II cells was measured after 60-hour culture. Data are pooled from two to three independent experiments, and bars represent means ± SEM (two-way ANOVA, Sidak's multiple comparison). *P < 0.5, ****P < 0.0001.

DCs (cDCs) (CD11c$^+$MHCII$^+$F4/80$^-$) can be divided into two subsets based on the expression of CD11b$^+$ (cDC2) and XCR1$^+$ (cDC1), with the CD11b$^+$ DC subset representing the dominant DC population during the steady state (Fig. 1, D and E). Although the XCR1$^+$ cDC1 subset is considered a uniform lineage (*4*), the CD11b$^+$ cDC2 subset is heterogenous, containing subpopulations of DCs with diverse functional properties (*5*). Consistent with previous studies (*6*), we can identify two subpopulations of cDC2 in the NALTs,

including $CD103^+CD11b^+$ DCs (cDC2) and $CD103^-CD11b^+$ DCs (cDC2) (Fig. 1E). A small population of plasmacytoid DCs was also present in the NALTs during the steady state (fig. S1). To assess the ability of NALT DC subsets to present inhaled antigen and induce T cell activation, we infected mice in the URT with a recombinant influenza A virus (x31) that expressed either the CD8 (SIINFEKL; x31-OVA_1) (*7*) or CD4 (ISQAVHAAHAEINEAGR; x31-OVA_2) (*8*) epitope from the model antigen ovalbumin (OVA). On days 1 to 4 after infection, DC subsets sort-purified from cLN and NALT were assessed directly ex vivo for their ability to stimulate $CD8^+$ OT-I or $CD4^+$ OT-II cell proliferation. In the cLN, the $XCR1^+$ DC subset was responsible for most of the MHCI (major histocompatibility complex class I) presentation to $CD8^+$ OT-I cells after x31-OVA_1 infection (Fig. 1F), and the $CD11b^+$ DC subset mediated most of the MHCII presentation to $CD4^+$ OT-II cells after x31-OVA_2 infection (Fig. 1H). In contrast, no MHCI or MHCII antigen presentation was mediated by $CD11b^+$ DCs recovered from the NALTs (Fig. 1, G and I).

The inability of NALT DCs to present viral antigen directly ex vivo is not merely a result of insufficient delivery of antigen to this structure, as we have previously reported that a large number of influenza antigen-positive cells are present in the NALTs during the acute phase of an influenza virus infection (*9*). Hence, we speculated that NALT DCs have an impaired antigen presentation capacity. To investigate this further, we assessed the ability of purified NALT DC subsets to present antigen sourced in vitro. Analysis of the $XCR1^+$ NALT DC subset was hampered by its rarity. To overcome this, we injected mice with a B16 melanoma cell line that secretes Flt3-L, a key cytokine involved in DC differentiation, previously shown to successfully boost the number of $XCR1^+$ DCs within the NALT (*6*). Sort-purified $CD11b^+$ and $XCR1^+$ DC populations from the NALTs and cLN of B16-Flt3-L–treated mice were incubated with carboxyfluorescein diacetate succinimidyl ester (CFSE)–labeled OT-I or OT-II cells together with irradiated OVA-coated splenocytes (OCSs), which served as a source of antigen. Proliferation of the T cells, measured as a loss of CFSE fluorescence, was quantitated 60 hours later by flow cytometry. Although both the $CD11b^+$ and $XCR1^+$ DC subsets isolated from the cLN were able to present cell-associated antigen and drive OT-I and OT-II proliferation, neither DC subset recovered from the NALT was able to promote proliferation of either T cell population (Fig. 1, J to L).

To further investigate why NALT DCs might be incapable of driving T cell proliferation, we checked a variety of important DC functions and attributes in these cells including (i) up-regulation of activation markers, (ii) morphology, (iii) cytokine production, and (iv) ability to uptake and process antigen. NALT DCs, similar to cLN DCs, up-regulated expression of MHCII, CD80, and CD86 after in vitro activation (Fig. 2, A and B) and microscopically displayed characteristic dendritic morphology (Fig. 2C). We observed no significant difference in the ability of NALT and cLN DCs to produce interleukin-12 (IL-12) (p40/p70) after in vitro stimulation (Fig. 2, D and E) and found that DC subsets recovered from the NALTs and cLN captured comparable amounts of soluble antigen (OVA conjugated to the pH-insensitive fluorochrome Alexa Fluor 488) (Fig. 2, F to H). To test whether the defect in NALT DC antigen presentation was due to an impairment in antigen processing, sort-purified $CD11b^+$ DCs from the NALTs or cLN of mice were coated with OT-II peptide; this eliminated the need for the DCs to process the antigen because the peptide can bind directly to surface MHCII. Peptide-coated DCs were cultured with CFSE-labeled OT-II cells for 60 hours. Whereas peptide-pulsed $CD11b^+$ DCs recovered from the cLN could drive OT-II expansion, NALT $CD11b^+$ DCs coated in OT-II peptide did not efficiently drive T cell proliferation (Fig. 2I). Together, these results show that DCs recovered from the NALTs during the steady state are defective at priming T cell responses.

NALT DCs suppress T cell proliferation

In addition to playing a pivotal role in antigen presentation to drive T cell priming, DCs also have tolerogenic functions, participating in the maintenance of central and peripheral tolerance and in the resolution of ongoing immune responses (*10*). Because the DC populations present within the NALT were defective at inducing T cell priming, we next explored whether these DCs were tolerogenic. We first assessed the ability of NALT DCs to suppress T cell priming in vitro. To do this, $XCR1^+$ or $CD11b^+$ DCs sort-purified from the cLN of mice were incubated with CFSE-labeled OT-I or OT-II cells together with OCS (antigen) and adjuvant [lipopolysaccharide (LPS)] in the presence or absence of sort-purified bulk NALT DCs (5:1 cLN DC:NALT DCs), and proliferation was quantitated 60 hours later by flow cytometry. Both the $CD11b^+$ and $XCR1^+$ DC subsets isolated from the cLN were able to present cell-associated antigen and drive OT-I and OT-II proliferation in the absence of NALT DCs, but notably, when NALT DCs were added to the culture, T cell proliferation was completely abrogated (Fig. 3, A to C). To gain insight into the potency of suppression mediated by the NALT DCs and to determine whether there was a difference in suppressor activity between the $CD11b^+$ and $XCR1^+$ NALT DC subsets, we repeated the assay described above but this time introduced titrated numbers of $CD11b^+$ or $XCR1^+$ NALT DCs (ratio of 5:1, 10:1, or 20:1 cLN DC:NALT DCs). We found that both NALT DC subsets could effectively block OT-I and OT-II proliferation (Fig. 3, D and E) and this suppressive effect was potent, as only when NALT DCs were diluted to a 20:1 ratio (with cLN DCs) was T cell proliferation restored to levels observed in the controls (Fig. 3, D and E). In addition to blocking expansion of naïve T cells, we found that NALT DCs also blocked memory OT-I T cell proliferation (fig. S2, A and B). Moreover, NALT DCs could also suppress T cell proliferation when introduced into a mixed lymphocyte reaction (Fig. 3, F and G). To show this latter effect, responder CFSE-labeled T cells purified from C57BL/6 mice were cultured at a 1:1 ratio for 5 days with BALB/c irradiated stimulator cells either alone or with cLN DCs or NALT DCs (from C57BL/6 mice). Whereas C57BL/6 responder T cells could undergo robust expansion after coculture with BALB/c stimulator cells, uninfluenced by the addition of cLN DCs, the introduction of NALT DCs hindered responder T cell expansion (Fig. 3, F and G). Together, these findings indicate that NALT DCs can suppress naïve, memory, and allogenic T cell expansion.

Next, we determined whether DCs with suppressor activity were also present in other mucosal-associated lymphoid tissue and looked for these cells in Peyer's patches, the mucosal-associated lymphoid tissue that is associated with the gut. $XCR1^+$ or $CD11b^+$ DCs sort-purified from the cLN of mice were incubated with CFSE-labeled OT-I cells together with antigen in the presence or absence of titrated numbers of $CD11b^+$ or $XCR1^+$ NALT DCs, Peyer's patch DCs, or, as a control, splenic DCs (ratio of 5:1, 10:1, or 20:1 cLN DC:NALT, PP, or spleen DCs), and proliferation was quantitated 60 hours later by flow cytometry. We found that only the DCs

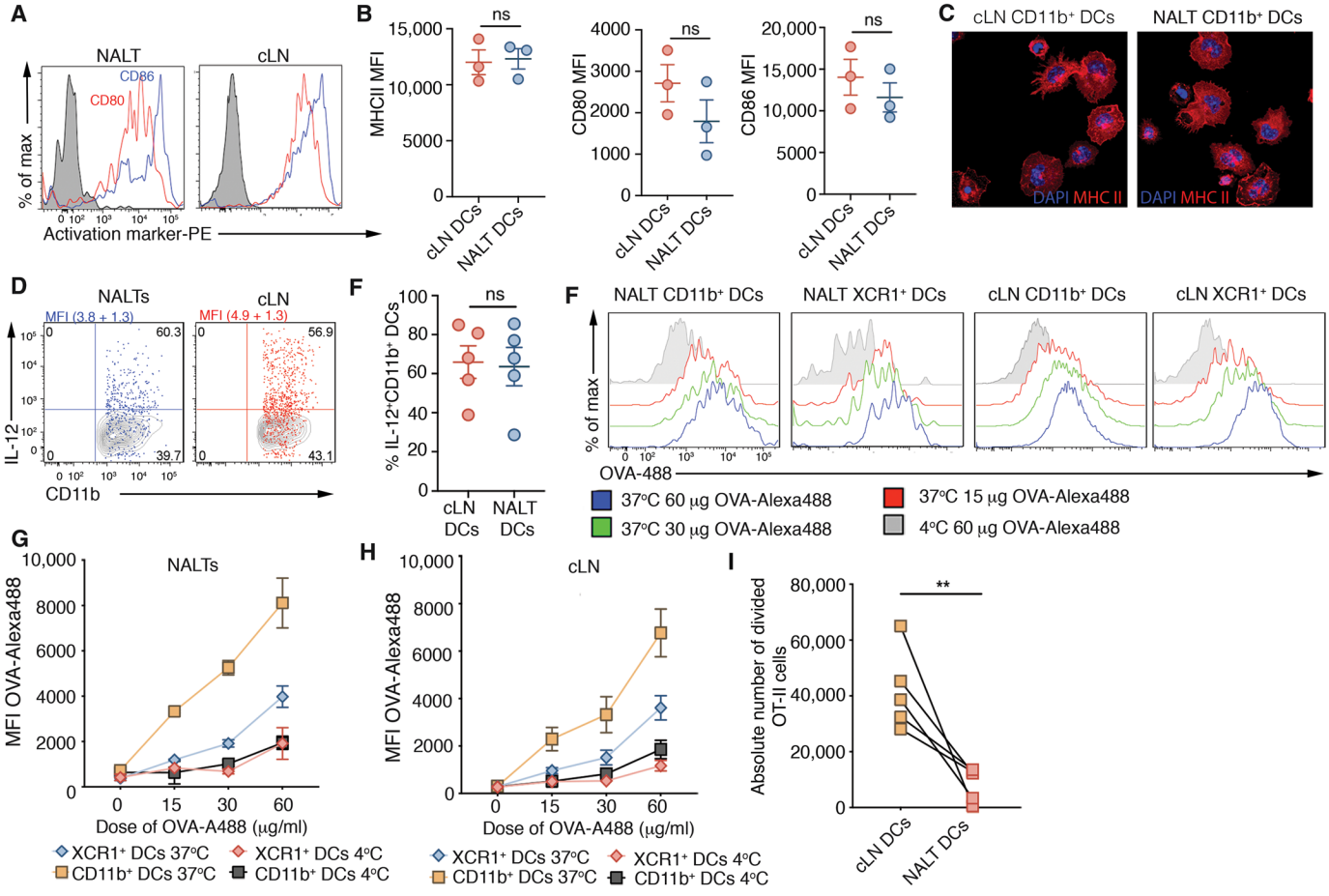

Fig. 2. DCs in the NALTs are capable of maturation, cytokine production, and antigen uptake. (**A** and **B**) Expression levels of MHCII, CD86, and CD80 on CD11b$^+$ NALT DCs and CD11b$^+$ cLN DC activated for 12 hours with LPS. (A) Representative histograms depicting the level of expression of CD86 and CD80. Gray histogram represents unstained control. (B) Mean fluorescence intensity (MFI) of MHCII, CD80, and CD86. Bars represent means ± SEM. Data are pooled from three experiments (paired *t* test). (**C**) MHCII$^+$CD11c$^+$F4/80$^-$ DCs from the cLN and NALTs were sort-purified, and cellular morphology was analyzed by immunohistochemistry staining for MHCII (M5/114, red) and the nuclear dye DAPI (blue). Data are representative of two independent experiments. (**D** and **E**) Representative flow cytometry profiles gated on CD11b$^+$ DCs isolated from the NALTs and cLN depicting the level of expression of IL-12 after 6 hours of in vitro activation in the presence of LPS (dot plots). Contour plots indicated IL-12 unstimulated samples. The average fold increase in MFI of IL-12 (stimulated samples relative to unstimulated control samples) is enumerated. Data are pooled from five experiments (means ± SEM). (E) Percentage of IL-12–producing DCs. Bars represent means ± SEM. Data are pooled from five experiments (paired *t* test). (**F** to **H**) Purified DCs isolated from the NALTs and cLN were incubated with the indicated concentrations of OVA–Alexa Fluor 488 (OVA-A488) for 45 min at 4° or 37°C. (F) The histograms show uptake of antigen by the CD11b$^+$ and XCR1$^+$ DC subsets. (G and H) Endocytosis was measured as an increase in mean linear fluorescence. The graphs show means ± SEM. Data are pooled from two to three experiments. (**I**) Proliferation of CFSE-labeled OT-II cells cultured for 60 hours together with OT-II peptide–loaded CD11b$^+$ DC isolated from cLN or NALTs. The absolute number of divided OT-II cells was measured after 60-hour culture. Data are pooled from five independent experiments (Mann-Whitney *U* test). ns, not significant. $^{**}P < 0.01$.

isolated from the NALTs could suppress T cell proliferation (fig. S2, C and D). Thus, suppressor activity is not a universal trait of DCs present within mucosal-associated lymphoid tissue. Moreover, it was only the DC subset present within the NALTs that displayed this suppressor activity, because "non-DCs" (MHCII$^+$CD11c$^-$) isolated from the NALTs (fig. S2E), and DCs recovered from the nasal tissue (fig. S2E), had no significant impact on T cell expansion. We next explored whether, in addition to suppressing T cell activation, NALT DCs could alter T cell polarity and preferentially induce the development of regulatory T cells (T_{regs}). NALT DCs coated with the OT-II peptide did not preferentially drive the development of Foxp3$^+$ T_{regs} (fig. S3, A and B). Furthermore, although NALT DCs suppressed OT-II proliferation when introduced into cultures with cLN DCs, OT-II cells, and antigen, they did not affect the frequency of Foxp3$^+$ T_{reg} development (fig. S3, C and D).

We next examined whether NALT DCs were blocking T cell activation by abrogating the antigen presentation ability of the conventional cLN DCs. We first tested the possibility that NALT DCs were affecting the capacity of the cLN DCs to undergo maturation. This was not the case, as the expression levels of activation markers CD86 and MHCII on LPS-stimulated cLN DCs were unimpaired by the presence of NALT DCs (fig. S4, A and B). Next, we determined whether NALT DCs were affecting the capacity of the cLN DCs to uptake, process, and present antigen. To this end, we coated XCR1$^+$ or CD11b$^+$ DCs, which were sort-purified from the cLN of mice with OT-II peptide, and cultured these peptide-loaded DCs with CFSE-labeled CD4$^+$ OT-II in the presence or absence of NALT DCs. In this scenario, where we removed the requirement of the cLN DCs to capture and process the antigen, we still observed that NALT DCs could block OT-II CD4$^+$ T cell expansion (fig. S4C). Last, we

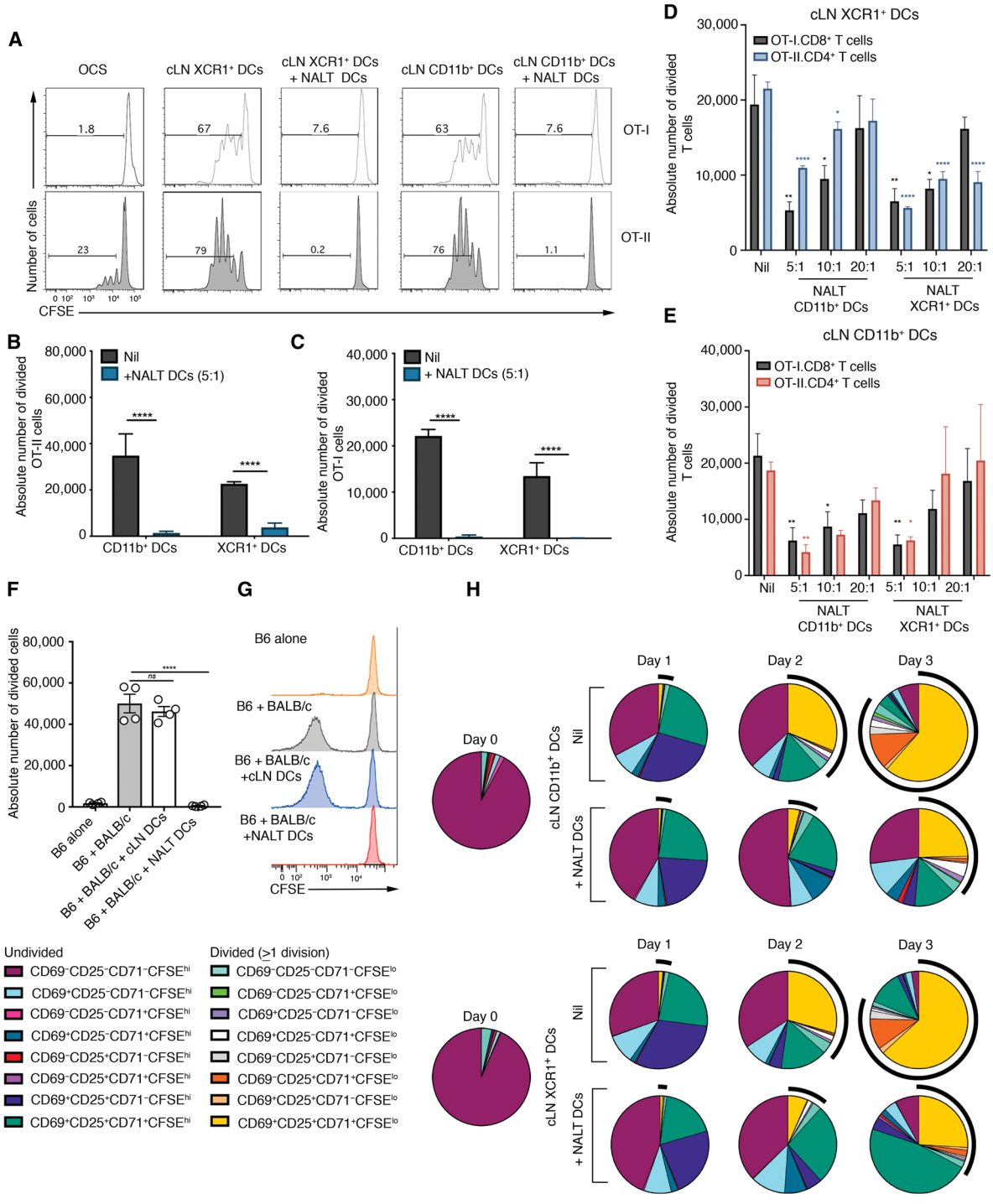

Fig. 3. NALT DCs suppress T cell proliferation but not activation. (**A** to **C**) Proliferation of CFSE-labeled OT-I or OT-II cells cultured for 60 hours together with OCS, CD11b$^+$, or XCR1$^+$ DCs isolated from cLN, either alone (Nil) or with NALT DCs (5:1 ratio). (A) Representative histograms of CFSE dilution of OT-I and OT-II cells after 60-hour culture. The absolute number of divided (B) OT-II and (C) OT-I cells was measured after 60-hour culture. Data are pooled from three independent experiments, and bars represent means ± SEM (two-way ANOVA, Sidak's multiple comparison). (**D** and **E**) Proliferation of CFSE-labeled OT-I and OT-II cells cultured for 60 hours together with OCS and (D) XCR1$^+$ or (E) CD11b$^+$ DCs isolated from cLN, either alone (Nil) or with the indicated numbers of NALT DC subsets. The absolute number of divided OT-I or OT-II was measured after 60-hour culture. Data are pooled from three to eight independent experiments per condition, and bars represent means ± SEM (one-way ANOVA, Dunnett's multiple comparison). (**F** and **G**) Proliferation of CFSE-labeled responder B6 T cells cultured for 5 days together with irradiated BALB/c cells and either cLN or NALT DCs. (F) Absolute number of divided cells. Data are pooled from four experiments, dot represents individual experiments, and bars represent means ± SEM (two-way ANOVA, Sidak's multiple comparison). (G) Representative histograms of CFSE dilution of responder T cells after 5 days of culture. (**H**) OT-I cells cultured for 0 to 3 days together with OCS, CD11b$^+$, or XCR1$^+$ DC subsets isolated from cLN alone (Nil) or with NALT DCs (5:1 ratio). Pie charts represent the mean proportion of OT-I cells expressing listed combinations of markers. Data are pooled from three independent experiments. Black outer circles highlight the proportion of divided (CFSE^{lo}) cells. *P < 0.5, **P < 0.01, and ****P < 0.0001.

mixed NALT DCs with T cells that were activated via anti-CD3/28 cross-linking (i.e., independent of DC presentation) and observed reduced T cell proliferation (fig. S4D). Collectively, these findings suggest that NALT DCs were not suppressing T cell proliferation by merely abrogating the antigen presentation capacity of the cLN DCs.

To identify the stage within the T cell activation cycle that NALT DCs were instigating their block, cLN XCR1$^+$ or CD11b$^+$ DCs were incubated with CFSE-labeled OT-I cells together with antigen (OCS) in the presence or absence of sort-purified NALT DCs (5:1 cLN DC:NALT DCs), and proliferation (loss of CFSE) and expression of the T cell activation markers CD25, CD69, and CD71 were measured 24, 48, and 72 hours later by flow cytometry. At 24 hours after culture, T cells activated in the presence of NALT DCs up-regulated early activation markers similar to cells activated in the absence of these suppressor cells (Fig. 3H and fig. S5, A to C). Although the OT-I cells stimulated in the absence of NALT DCs entered cell cycle and had undergone at least two rounds of division by 48 hours after culture, the OT-I cells stimulated in the presence of NALT DCs were largely undivided and remained in this state for the duration of the experiment (Fig. 3H and fig. S5, A to C). To gain further insight into the fate of T cells interacting with NALT DCs, we cultured naïve OT-I T cells with XCR1$^+$ or CD11b$^+$ DC subsets purified from the NALTs or, as controls, matched DC subsets recovered from the cLN or spleen and monitored T cell survival. Whereas minimal cell death was observed when T cells were cultured with splenic or cLN DC subsets, we observed 50% fewer viable T cells after culture with either NALT DC subset (fig. S5D). Thus, T cells stimulated in the presence of NALT DCs up-regulate the expression of early activation markers, but fail to undergo robust proliferation and, instead, succumb to cell death.

NALT DCs suppress T cell proliferation via a contact-independent mechanism involving the production of PGE_2 and ROS

To gain insight into how NALT DCs were blocking T cell proliferation, we next assessed whether suppression required physical contact between the NALT DCs and the target cell. To this end, we used a transwell system where XCR1$^+$ or CD11b$^+$ cLN DCs, CFSE-labeled OT-I cells, and antigen (OCS) were placed into one chamber, and the NALT DCs were placed in the other. We quantitated T cell proliferation 60 hours later and found that physical separation of NALT DCs from the other constituents of the presentation assay did not affect their ability to impede T cell proliferation (Fig. 4A). We observed comparable levels of inhibition when NALT DCs were either mixed with the other cellular components of the assay or separated by a transwell, suggesting that the inhibitory effect was contact independent. To further validate that a factor released by the NALT DCs was responsible for blocking T cell activation, we collected the supernatant from sort-purified NALT DCs or, as a control, NALT non-DCs cultured for 24 hours in vitro. Supernatants were spiked into a well with XCR1$^+$ or CD11b$^+$ cLN DCs, CFSE-labeled OT-I cells, and antigen (OCS). The addition of the supernatant from the NALT "non-DC" culture did not affect T cell proliferation, but the supernatant from the NALT DC culture alone could attenuate T cell proliferation (Fig. 4B). Hence, NALT DCs block T cell proliferation via a mechanism that does not require cell contact.

RNA sequencing (RNA-seq) analysis was performed on CD11b$^+$ and XCR1$^+$ DCs sort-purified from the NALTs and cLN of naïve mice to identify a transcriptional profile that could explain the suppressive nature of these cells. The CD11b$^+$ and XCR1$^+$ DCs recovered from both the cLN and NALTs expressed hallmark DC subset signature genes (fig. S6, A to D) (*5*, *11*), and although most of the genes, including those encoding toll-like receptors (fig. S6E), were equivalently expressed between the same subset of DC present within both lymphoid compartments, there were several interesting discrepancies (Fig. 4, C to E). Comparing matched CD11b$^+$ and XCR1$^+$ DC subsets, we identified 1025 and 1923 differentially expressed genes, respectively. When comparing cLN and NALT DC subsets, some of the most differentially expressed genes were mitochondrial genes. An elevation of mitochondrial genes can be linked to cell death; however, before transcriptional analysis, we confirmed that each DC subset was >99% viable. In addition to being associated with cell death, differential expression of mitochondrial genes can also be indicative of differences in metabolism. We found that six subunits of the NADH (reduced form of nicotinamide adenine nucleotide) dehydrogenase (ND1 to ND6), cytochrome b, and cytochrome c oxidase subunits (COX) 1 to 3 were elevated in both NALT DC subsets compared with their matched subsets recovered from the cLN (Fig. 4F); these genes encode for proteins that constitute members of complex I (ND1 to ND6), complex III (cytochrome b), and complex IV (COX1 to COX3) of the mitochondrial electron transport chain. Elevated expression of these complexes is indicative of increased oxidative phosphorylation (OXPHOS), a metabolic signature previously associated with tolerogenic human DCs (*12*). In addition to being involved in respiratory electron transport and adenosine triphosphate (ATP) synthesis, the mitochondrial electron transport chain generates ROS. After a brief in vitro stimulation, we confirmed that CD11b$^+$ and XCR1$^+$ DC subsets isolated from the NALTs expressed elevated levels of ROS compared with their matched subsets recovered from the cLN (Fig. 4, G and H).

Exposure of T cells to high concentrations of ROS has a negative impact on T cell activation and survival, resulting in (i) T cell apoptosis (*13*–*15*), (ii) down-regulation of the expression of T cell receptor (TCR) ζ chain, leading to impaired TCR signaling (*15*, *16*), and (iii) nitrosylation of the TCR, resulting in T cell anergy (*17*). Furthermore, many studies using a variety of cell types show that increased intracellular ROS can lead to the expression of cyclooxygenase-2 (Cox-2) (*18*–*21*), a key enzyme that promotes the synthesizes of PGE_2, which is a lipid mediator known to inhibit T cell proliferation (*22*). After a 6-hour in vitro stimulation, CD11b$^+$ DCs isolated from the NALTs expressed higher levels of Cox-2 compared with matched subsets recovered from the cLN (fig. S7, A and B) and higher concentrations of PGE_2 could be detected in the supernatants of cultured NALT DCs compared with matched subsets isolated from the cLN (fig. S7C). Because both ROS and PGE_2 have previously been shown to impair T cell proliferation, we explored whether these factors were responsible for the suppressor activity of NALT DCs. To do this, we tested whether inhibitors that block ROS [*N*-acetylcysteine (NAC)] and cyclooxygenase activity (indomethacin) could restore T cell expansion when introduced into our in vitro antigen presentation assay. XCR1$^+$ or CD11b$^+$ DCs sort-purified from the cLN of mice were incubated with OCS in the presence or absence of NALT DCs (5:1 cLN DC:NALT DCs) with either 10 μM indomethacin, 0.5 mM NAC, or both reagents. To avoid the inhibitors having a direct effect on the T cells, CFSE-labeled OT-I cells were added 24 hours later and proliferation was measured after 60 hours of in vitro culture. Without the introduction of the inhibitors, NALT DCs reduced T cell expansion to 31% of that observed in the absence of these cells, and although the introduction of these inhibitors individually mildly

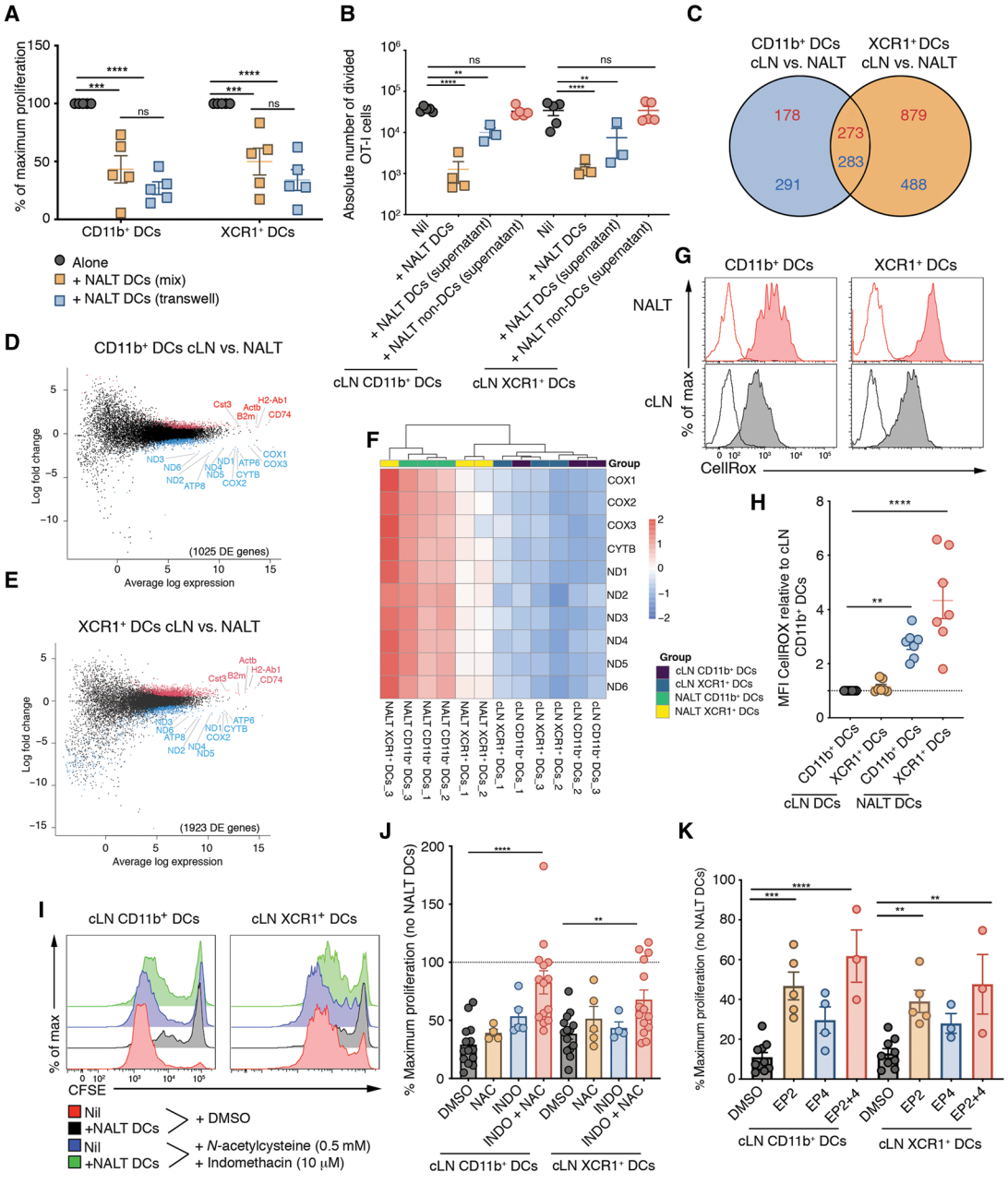

Fig. 4. NALT DCs suppress T cell proliferation via the production of PGE_2 and ROS. (**A**) Proliferation of CFSE-labeled OT-I cells cultured for 60 hours together with OCS, CD11b$^+$, or XCR1$^+$ cLN DCs, either alone (alone) or with bulk NALT DC (5:1), which were added directly to the well (mix) or seeded onto a transwell. Graphs depict the percentage of maximum proliferation. Data are pooled from five experiments, dot represents individual experiments, and lines represent means ± SEM (two-way ANOVA, Sidak's multiple comparison). (**B**) Proliferation of CFSE-labeled OT-I cells cultured for 60 hours together with OCS, CD11b$^+$, or XCR1$^+$ cLN DCs, either alone (Nil) or with NALT DCs (5:1), or the supernatant recovered from NALT DC or NALT non-DC cultures. Graphs depict the absolute number of divided OT-I cells after 60-hour culture. Data are pooled from three to five independent experiments, and bars represent means ± SEM (two-way ANOVA, Sidak's multiple comparison). (**C** to **F**) RNA-seq analysis performed on CD11b$^+$ and XCR1$^+$ DCs isolated from the NALTs and cLN of naïve mice. (C) Venn diagram comparing cLN versus NALT CD11b$^+$ DCs and cLN versus NALT XCR1$^+$ DCs, depicting the number of similarly regulated (red, up-regulated; blue, down-regulated) differentially expressed (DE) genes. (D) Mean-difference plot depicting the fold change in gene expression (log_2-transformed) between cLN and NALT CD11b$^+$ DCs against the average log expression of each gene [in counts per million (CPM), log_2-transformed]. Red and blue points indicate genes significantly enriched in DCs from the cLN or NALT DCs, respectively. Black dots represent nonenriched genes. (E) Mean-difference plot depicting the fold change in gene expression (log_2-transformed) between cLN and NALT XCR1$^+$ DCs against the average log expression of each gene (in CPM, log_2-transformed). Red and blue points indicate genes significantly enriched in DCs from the cLN or NALT DCs, respectively. Black dots represent nonenriched genes. (F) Heatmap of expression values for the COX1 to COX3, cytochrome b (CYTB), and ND1 to ND6 genes in CD11b$^+$ DCs and XCR1$^+$ DCs isolated from NALT and cLN (presented as normalized log_2 expression). (**G** and **H**) Representative histograms showing the production of ROS measured by CellROX staining of CD11b$^+$ and XCR1$^+$ DCs isolated from the NALTs (red) and cLN (gray). Unfilled lines represent CellROX unstained control. (H) Graph depicts the relative MFI of CellROX in each DC population compared with cLN CD11b$^+$ DCs. Dots represent individual experiments, data are pooled from seven independent experiments, and bars represent means ± SEM (one-way ANOVA, Dunnett's multiple comparison). (**I** and **J**) CD11b$^+$ or XCR1$^+$ cLN DCs were cultured with OCS, either alone (Nil) or with NALT DCs (5:1) in the presence of vehicle control [dimethyl sulfoxide (DMSO)], 0.5 mM NAC, or 10 μM indomethacin (INDO), or both, for 24 hours before the addition of CFSE-labeled OT-I cells, and T cell proliferation was assessed 60 hours later. (I) Representative histograms of CFSE dilution of OT-I cells after 60-hour culture. (J) Percentage of maximum proliferation (relative to cultures without NALT DCs). Data are pooled from 4 to 14 independent experiments per condition, dots depict individual experiments, and bars represent means ± SEM (one-way ANOVA, Dunnett's multiple comparison). (**K**) CD11b$^+$ or XCR1$^+$ DCs isolated from cLN were cultured with OCS and CFSE-labeled OT-I cells either alone (Nil) or with NALT DCs (5:1) in the presence of a vehicle control (DMSO), or 12.5 μM EP2 inhibitor, or 12.5 μM EP4 inhibitor, or both, and proliferation was assessed 60 hours later. Data are pooled from 3 to 10 independent experiments per condition, dots depict individual experiments, and bars represent means ± SEM (one-way ANOVA, Dunnett's multiple comparison). $^{**}P < 0.01$, $^{***}P < 0.001$, and $^{****}P < 0.0001$.

increased T cell expansion, the addition of these inhibitors together restored T cell expansion to 70 to 80% (XCR1$^+$ and CD11b$^+$ DCs, respectively) to levels observed in conditions without suppressor DCs (Fig. 4, I and J). Thus, blocking Cox-2 activity and scavenging ROS counteracts the suppressor activity of NALT DCs.

To directly address whether cyclooxygenase-induced synthesis of PGE_2 was responsible for the NALT DC–mediated T cell suppression, we checked whether blocking the receptors for this prostanoid would render T cells resistant to NALT DC–mediated suppression. PGE_2 signals via four receptors (EP1, EP2, EP3, and EP4), but only EP2 and EP4 are highly expressed on T cells, and the anti-proliferative effects of PGE_2 are thought to occur predominately via EP2 signaling (*22*). XCR1$^+$ or CD11b$^+$ DCs sort-purified from the cLN of mice were incubated with CFSE-labeled OT-I cells together with OCS in the presence or absence of NALT DCs (5:1 cLN DC:NALT DCs) and with inhibitors for either EP2 or EP4 or both. Proliferation of the OT-I cells was measured 60 hours later. We found that blocking the EP2 receptor alone was sufficient to relieve the suppression mediated by NALT DCs (Fig. 4K). Collectively, these data indicate that NALT DCs can suppress T cell proliferation via a contact-independent mechanism that can be diminished by blocking the actions of ROS and PGE_2.

Human tonsil DCs suppress T cell responses

The NALT of mice is considered analogous to the Waldeyer's ring in humans, which collectively includes the adenoid and tonsil tissue. We next investigated whether DCs recovered from human NALT were also poised to suppress T cell proliferation. We first characterized the DC populations present in adult human tonsil/adenoid tissue and found that two DC (HLA-DR$^+$CD11c$^+$CD14$^-$CD3$^-$CD19$^-$) subsets could be identified on the basis of the expression of the markers CD141$^+$ (cDC1, BDCA-3) and CD1c$^+$ (cDC2, BDCA-1) (Fig. 5A). Studies by others have previously demonstrated that human tonsil DCs show poor antigen presentation capacity (*23*), and here, we examined whether these cells were immunosuppressive. To test the suppressor activity of human tonsil/adenoid DCs, we used a mixed lymphocyte reaction and assessed the capacity of these DCs to alter responder T cell proliferation. To this end, moDCs [granulocyte-macrophage colony-stimulating factor (GM-CSF) DCs] generated from peripheral blood mononuclear cells (PBMCs) were cocultured with mismatched CFSE-labeled responder T cells and nontyped tonsil HLA-DR$^-$CD11c$^-$ cells (Nil), and to this, we introduced either (i) tonsil DCs (HLA-DR$^+$CD11c$^+$), (ii) tonsil non-DCs (HLA-DR$^+$CD11c$^-$), or (iii) as a control, spleen DCs (HLA-DR$^+$CD11c$^+$) (Fig. 5B). The absolute number of divided responder T cells was measured after 5 days of culture. The presence of tonsil DCs suppressed responder T cell proliferation by 50% of that observed in cultures that lacked these cells (Fig. 5, C to E). Furthermore, non-DC isolated from the tonsil tissue could not attenuate responder T cell expansion, nor could the addition of splenic DCs (Fig. 5, C to E). Thus, human tonsil DCs, like their murine counterparts, have the ability to suppress T cell proliferation.

Inflammation induced by pathogen exposure, but not commensal bacteria, changes the composition of DCs present within the NALTs, rendering the pool incapable of suppressing T cell responses

The data thus far imply that the default role for DCs in the NALT during the steady state is to suppress T cell responses, potentially as a means to prevent unwarranted immune activation against harmless antigens and bacterial commensals encountered at the nasopharyngeal mucosa. Using our mouse model, we next investigated whether infection/inflammation influenced the functionality and composition of DCs present within the NALTs. To do this, we first monitored changes in the number and composition of DCs in the NALTs over the course of an URT infection with influenza virus (x31). Although the number of XCR1$^+$ DCs in the NALTs did not change over the course of the infection, the number of CD11b$^+$ DCs declined for the first 2 days after infection but increased thereafter (Fig. 6A). Further profiling of the CD11b$^+$ DCs that accumulated in the NALTs from >day 2 after infection revealed that the vast majority of these DCs expressed CD64, the high-affinity immunoglobulin G (IgG) FcγR1, and stained with the MAR-1 antibody, which is directed against the high-affinity IgE FcεR1 (Fig. 6B). It has been demonstrated recently that the coexpression of these receptors distinguishes conventional CD11b$^+$ DCs from newly recruited moDCs (*24*). Whereas infection-induced inflammation appeared to recruit moDCs into the NALTs, and these cells represented the dominant DC population in this lymphoid tissue between days 4 and 10 after infection, by day 15 after infection, the composition of DCs within this structure returned to a steady-state profile (Fig. 6B). To confirm that this change in DC composition was due to an influx of moDCs rather than an alteration in the phenotype of preexisting DCs, we infected CCR2 knockout (KO) mice, which have impaired homing of inflammatory monocytes, the immediate precursors of moDCs, and found significantly less CD64$^+$CD11b$^+$ DCs within the NALTs on day 4 after infection (fig. S8). Next, we assessed whether the change in DC composition in the NALTs altered the suppressive nature of this lymphoid tissue. To this end, we sort-purified bulk DC populations from NALTs harvested from either naïve mice or mice that had been intranasally infected with influenza virus 4 or 15 days earlier. We cultured these cells with cLN XCR1$^+$ or CD11b$^+$ DCs recovered from naïve mice and CFSE-labeled OT-I cells together with cell-associated antigen (OCS). Consistent with our earlier experiments, NALT DCs sort-purified from naïve mice could suppress T cell proliferation (Fig. 6C). The DC pool recovered from the inflamed NALTs (day 4 after infection) no longer suppressed T cell proliferation, whereas those isolated from the NALTs during the recovery phase (day 15 after infection) had once again regained their suppressor activity (Fig. 6C). Our data suggest that the infiltration of moDCs alleviated the suppressive nature of the NALT DC pool. To confirm this hypothesis, we infected CCR2 KO mice with influenza virus (x31) and, on day 4 after infection, tested the immunomodulatory nature of the DCs as described above. In this scenario, the DCs recovered from the infected CCR2 KO mice remained immunosuppressive, indicating that the recruitment of moDCs is required to transform the NALT DC pool into a nonsuppressive population (Fig. 6C).

Our data show that infection with a respiratory pathogen (influenza virus) can alleviate the suppressive nature of the NALT DC pool. We next explored how exposure to commensal bacteria, commonly encountered at the nasopharyngeal mucosa, influenced the immunosuppressive nature of the DCs within the NALT. We infected mice in the upper airways with 10^8 colony-forming units (CFU) of *Staphylococcus aureus*, and this resulted in nasal bacterial colonization in about half of the mice for at least 21 days and evoked a very mild and transient inflammatory response, as measured by the level of inflammatory cytokines in the nasal lavage (Fig. 6, D and E).

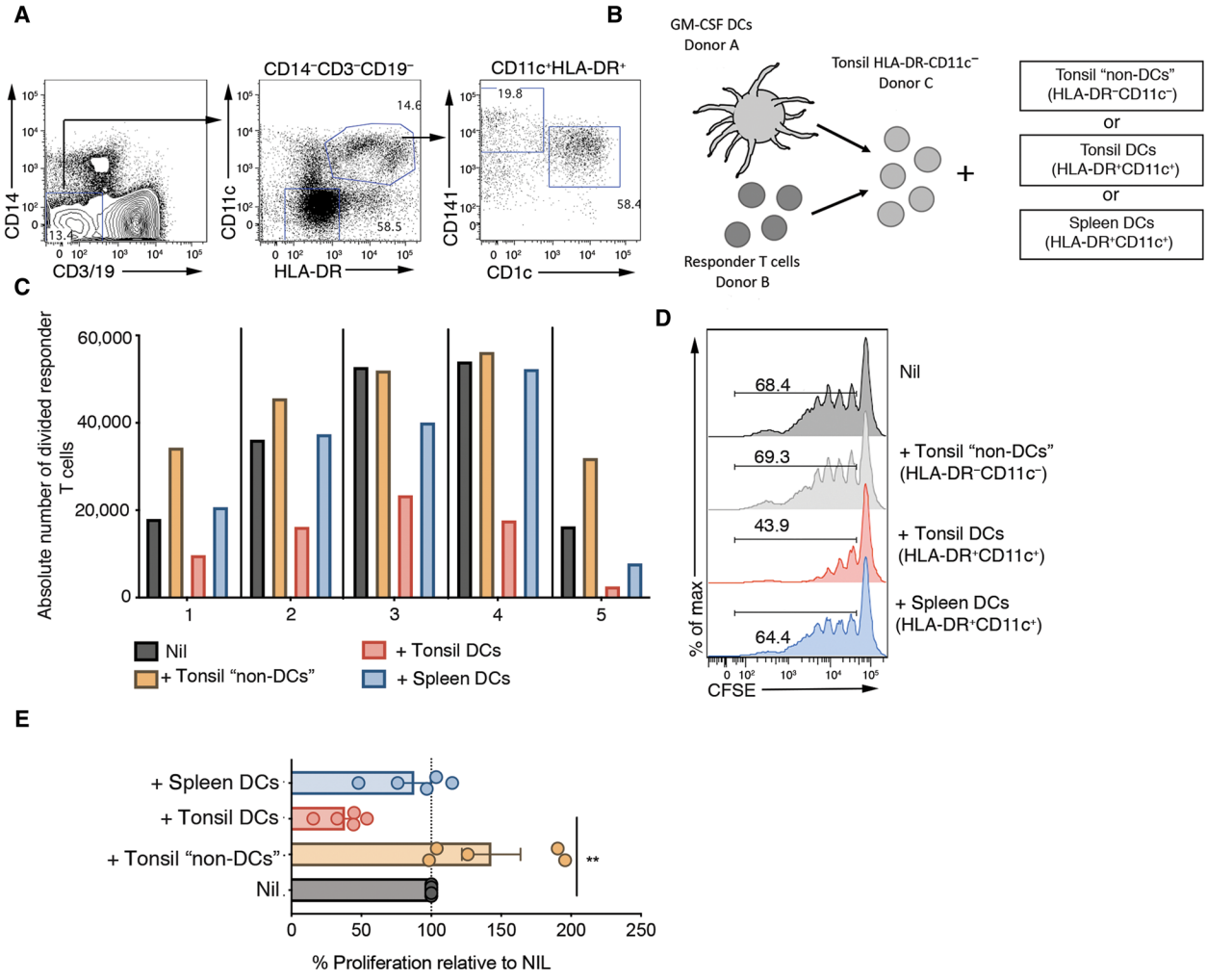

Fig. 5. Human tonsil DCs suppress T cell responses. (**A**) Representative flow cytometry profiles gated on DCs ($CD14^-CD3^-CD19^-CD11c^+HLA\text{-}DR^+$) depicting the proportion of $CD141^+$ and $CD1c^+$ subsets in human tonsil tissue. (**B** to **E**) Mixed lymphocyte reaction (MLR), where moDCs differentiated from PBMCs were cocultured with mismatched CFSE-labeled responder T cells, tonsil $HLA\text{-}DR^-CD11c^-$ cells (Nil), and either tonsil non-DCs ($HLA\text{-}DR^-CD11c^-$), tonsil DCs ($HLA\text{-}DR^+CD11c^+$), or spleen DCs ($HLA\text{-}DR^+CD11c^+$). The absolute number of divided cells was measured after 5 days of culture. (B) Schematic diagram of MLR assay. (C) Absolute number of divided responder T cells after 5 days of culture. Five independent experiments using five different tonsil donors are shown. (D) Representative histograms of CFSE dilution of responder T cells after 5 days of culture. (E) Percentage of proliferation relative to Nil. Data are pooled from five independent experiments, dots depict individual experiments, and bars represent means ± SEM (one-way ANOVA, Dunnett's multiple comparison). $^{**}P < 0.01$.

We observed no significant increase in the number of moDCs within the NALTs of *S. aureus*–infected mice (Fig. 6F), and, unlike the DC pool present in the NALTs of mice acutely infected with influenza virus, which lost their immunomodulatory activity, DCs sort-purified from the NALTs of *S. aureus*–infected mice remained immunosuppressive (Fig. 6G). Collectively, these data show that DCs in the NALTs retain suppressor activity after exposure to commensal bacteria.

We next examined how the influx of moDCs was alleviating the suppressive nature of the NALT DC pool and tested whether moDCs were simply diluting out the suppressive DC population or whether they were altering the immunomodulatory nature of the NALT DCs. To this end, we intranasally infected mice with influenza virus and purified NALT moDCs ($MAR\text{-}1^+CD64^+$) and conventional $CD11b^+$ DCs ($MAR\text{-}1^-CD64^-$) 4 days later. At this time, moDCs represented >70% of the bulk DC pool within the inflamed NALTs. We cultured these NALT DC subsets with cLN $XCR1^+$ or $CD11b^+$ DCs recovered from naïve mice and CFSE-labeled OT-I cells together with cell-associated antigen (OCS) and measured T cell proliferation 60 hours later. Consistent with earlier experiments testing the suppressive activity of bulk NALT DCs during influenza virus infection (Fig. 6C), we find that the purified moDC population recovered from the NALTs of virus-infected mice did not suppress T cell proliferation (Fig. 6, H and I). The conventional $CD11b^+$ DC population isolated from the inflamed NALT retained their suppressor activity (Fig. 6, H and I). Together, these findings imply that inflammatory moDCs alleviate the suppressive nature of the NALT DC pool by diluting out the suppressive DC population.

Sustained antigen release into the URT improves T cell responses in the NALTs

To test whether the altered composition of DCs within the inflamed NALTs was capable of priming T cell responses, we immunized mice in the upper airways with a live attenuated influenza virus vaccine

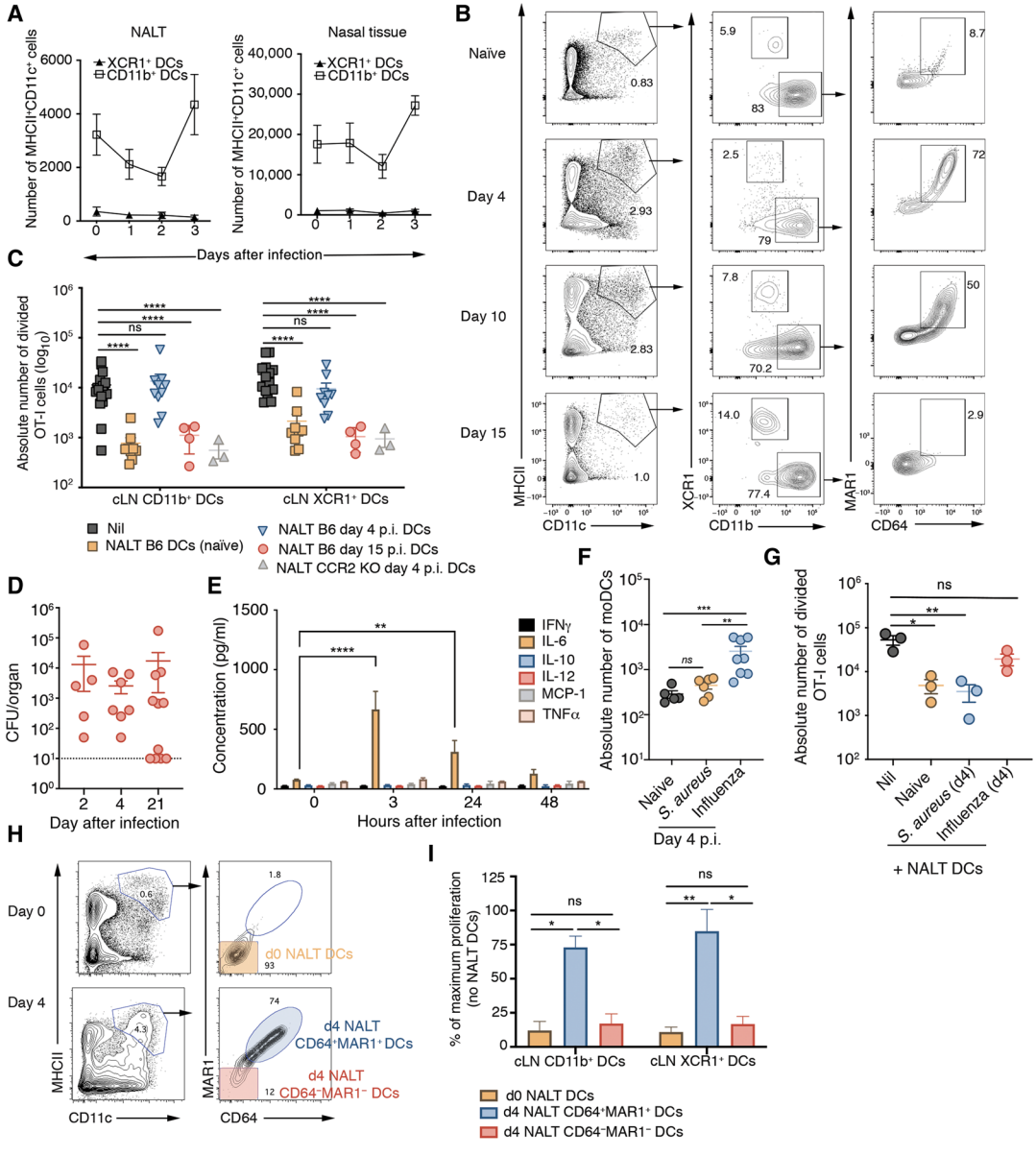

Fig. 6. Inflammation induced by pathogen exposure, but not commensal bacteria, changes the composition of DCs present within the NALT, rendering the pool incapable of suppressing immune responses. (**A**) Absolute number of CD11b$^+$ and XCR1$^+$ DCs in the NALTs and nasal tissue at the indicated days after intranasal infection with 10^4 PFU of influenza virus (x31). Data are pooled from three independent experiments, with the symbols representing means ± SEM ($n = 6$ to 13 mice per group). (**B**) Representative flow cytometry profiles gated on MHCII$^+$CD11c$^+$ F4/80$^-$ DCs isolated from the NALTs of naïve mice or mice 4, 10, and 15 days after intranasal infection, with influenza virus (x31) depicting the change in composition of DC subsets (CD11b$^+$, XCR1$^+$, and CD11b$^+$CD64$^+$MAR-1$^+$). (**C**) Proliferation of CFSE-labeled OT-I cells cultured for 60 hours together with OCS, CD11b$^+$, or XCR1$^+$ cLN DC subsets, either alone or with NALT DCs (5:1) isolated from either naïve mice, or B6 or CCR2 KO mice infected 4 or 15 days before with 10^4 PFU influenza virus (x31). The absolute number of divided OT-I cells was measured after 60-hour culture. Data are pooled from 3 to 14 independent experiments per condition, dots depict individual experiments, and bars represent means ± SEM (two-way ANOVA, Sidak's multiple comparison). p.i., post infection. (**D**) Mice were infected intranasally with 10^8 CFU of *S. aureus*, and 2, 4, and 21 days later, the bacterial load in the nose was measured. Symbols represent individual mice, and horizontal bars represent means ± SEM ($n = 5$ to 11 mice per time point). Dotted lines represent the limit of detection. (**E**) Mice were infected intranasally with 10^8 CFU of *S. aureus*, and at the indicated times, the level of a panel of cytokine/chemokines in the nasal lavage was measured by cytometric bead array. Bars represent means ± SEM ($n = 3$ to 11 mice per time point; one-way ANOVA, Sidak's multiple comparison). (**F**) Absolute number of moDCs (MHCII$^+$CD11c$^+$ CD11b$^+$CD64$^+$MAR-1$^+$) in the NALTs of B6 mice on day 4 after intranasal infection with influenza virus (x31) or *S. aureus*. Data are pooled from two independent experiments. Symbols represent individual mice, with lines representing means ± SEM ($n = 5$ to 8 per group, one-way ANOVA, Tukey's multiple comparison). (**G**) Proliferation of CFSE-labeled OT-I cells cultured for 60 hours together with OCS, CD11b$^+$ DCs isolated from cLN, either alone (Nil) or with NALT DCs (5:1) isolated from either naïve B6 mice, or B6 mice infected 4 days before with either influenza virus or *S. aureus*. The absolute number of divided OT-I cells was measured after 60-hour culture. Data are pooled from three independent experiments. Dots represent independent experiments, and lines represent means ± SEM (two-way ANOVA, Sidak's multiple comparison). (**H** and **I**) Proliferation of CFSE-labeled OT-I cells cultured for 60 hours together with OCS, CD11b$^+$, or XCR1$^+$ cLN DCs, either alone or with moDCs (CD64$^+$MAR1$^+$) or cDCs (CD64$^-$MAR1$^-$) (ratio 5:1) isolated from NALTs of either naïve mice, or B6 mice infected 4 days before with 10^4 PFU influenza virus (x31). The percentage of maximum proliferation (relative to cultures without NALT DCs) is shown. Data are pooled from three independent experiments. Bars represent means ± SEM (two-way ANOVA, Sidak's multiple comparison). IFNγ, interferon-γ; MCP-1, monocyte chemoattractant protein–1; TNFα, tumor necrosis factor–α. *$P < 0.5$, **$P < 0.01$, ***$P < 0.001$, and ****$P < 0.0001$.

(LAIV), and 4 days later, a time point when inflammatory moDCs would have accumulated in the NALTs, we intranasally administered OVA protein. As a control, we administered LAIV and OVA together at $t = 0$ hours. One hour after the administration of OVA protein, we recovered the NALTs, sort-purified the DC subsets, and cultured these cells with CFSE-labeled OT-I T cells to measure the antigen presentation capacity of these DCs directly ex vivo (Fig. 7A). Although we observed poor antigen presentation mediated by DCs recovered from uninflamed NALTs (d0 LAIV), we found that delaying the delivery of the OVA protein until day 4 after LAIV immunization

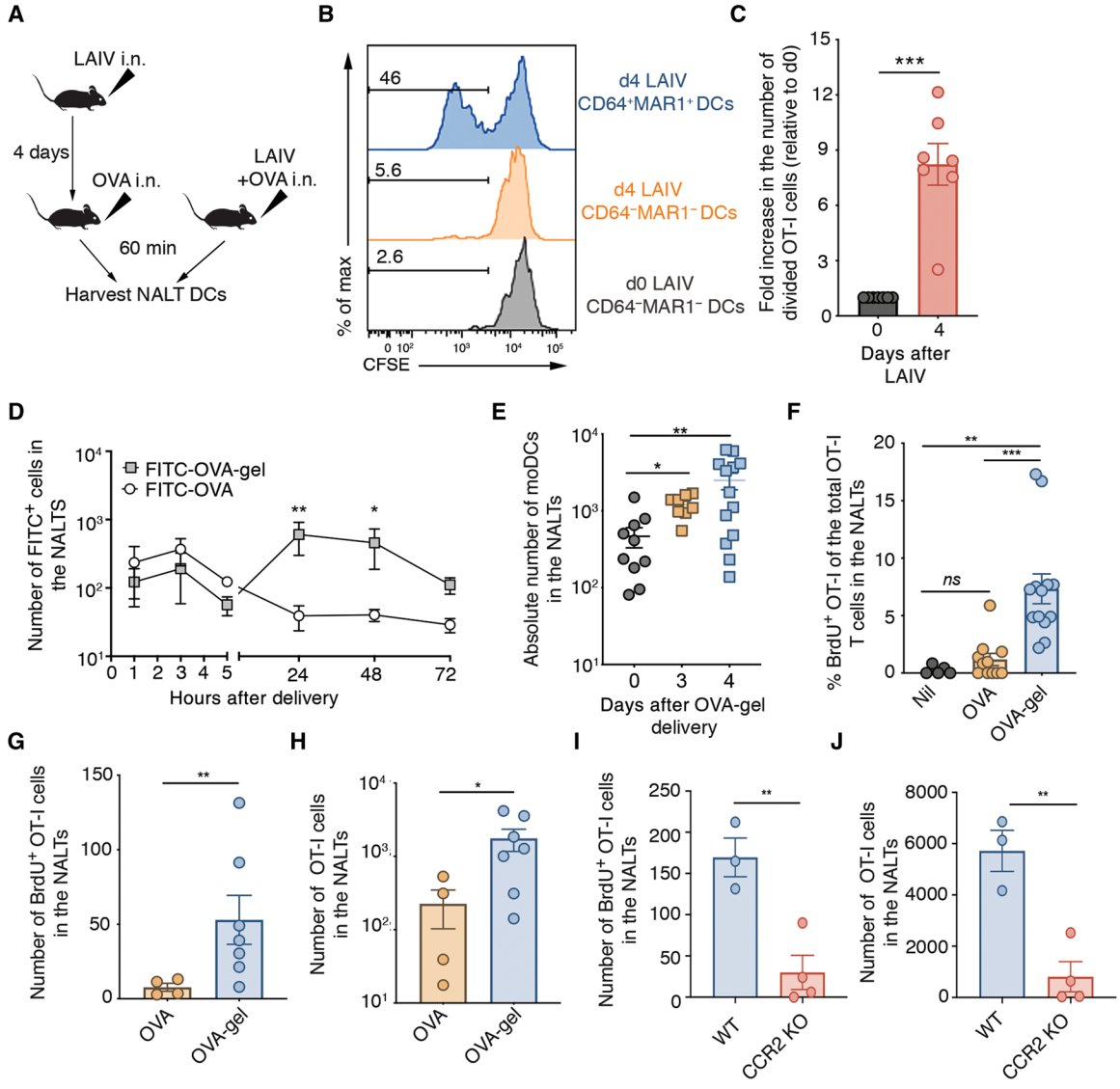

Fig. 7. Sustained antigen release into the URT improves T cell responses in the NALTs. (**A** to **C**) Proliferation of CFSE-labeled OT-I cells cultured for 60 hours together with DC subsets isolated from NALTs of mice immunized either 0 or 4 days earlier with LAIV and administered OVA protein 1 hour before harvest. (A) Schematic representative of the experimental approach. i.n., intranasally. (B) Representative histograms gated on OT-I cells depicting level of CFSE dilution. (C) Fold increase in the number of divided OT-I cells after 60-hour culture with d4 NALT moDCs relative to d0 NALT DCs. Data are pooled from seven experiments (paired *t* test). (**D**) Absolute number of FITC$^+$ cells in the NALTs at the indicated times after intranasal delivery of FITC-OVA or FITC-OVA-gel. Data are pooled from two independent experiments, and symbols represent means ± SEM ($n = 2$ to 6 mice per group; two-way ANOVA, Sidak's multiple comparison). (**E**) Absolute number of CD64$^+$ moDCs in the NALTs 3 and 4 days after intranasal delivery of OVA-gel. Data are pooled from two independent experiments. Symbols represent individual mice ($n = 8$ to 13 mice per group; one-way ANOVA, Dunnett's multiple comparison). (**F**) Proportion of BrdU$^+$ OT-I cells in the NALTs of memory mice (generated as described in Materials and Methods) 3 days after the delivery of either OVA or OVA-gel. Data are pooled from three independent experiments, with dots depicting individual mice and bars representing means ± SEM ($n = 5$ to 13 mice per group; one-way ANOVA, Tukey's multiple comparison). (**G** and **H**) Absolute number of (G) BrdU$^+$ OT-I and (H) total OT-I T cells in the NALTs on day 3 after OVA or OVA-gel delivery. Data are pooled from two independent experiments, with dots depicting individual mice and bars representing means ± SEM ($n = 4$ to 8 mice per group; unpaired *t* test). (**I** and **J**) Absolute number of (I) BrdU$^+$ OT-I and (J) total OT-I T cells in the NALTs of wild-type (WT) or CCR2 KO memory mice (generated as described in Materials and Methods) 3 days after the delivery of OVA-gel after a 1-hour BrdU pulse. Bars represent means ± SEM ($n = 3$ to 4 mice per group; unpaired *t* test). *$P < 0.5$, **$P < 0.01$, and ***$P < 0.001$.

boosted the capacity of the DCs recovered from the NALTs by about eightfold to prime T cell responses directly ex vivo (Fig. 7, B and C). Moreover, it was the newly recruited inflammatory moDC (CD64$^+$MAR-1$^+$) subset that was mediating this presentation. Together, these data indicate that local inflammation in the NALT results in the influx of moDCs, which transform this lymphoid tissue into an environment that can support the initiation of cellular immune responses.

Our data have important implications for intranasal vaccines that attempt to evoke cellular immunity. Our results suggest that an intranasal vaccine that aims to elicit a T cell response should induce the recruitment of moDCs into the NALTs and maintain antigen within this region until these immunogenic DCs arrive. Thus, we tested an intranasal vaccine delivery system that accommodated these requirements for its capacity to evoke T cell responses in the NALTs. Chitosan hydrogels are a sustained release vaccine delivery

system primarily consisting of the naturally occurring polymer chitosan (*25*). Chitosan solutions can be made thermosensitive with the addition of polymers such that the hydrogels only form as a result of an increase in temperature (*26*). This behavior can be exploited to produce chitosan solutions that are liquids at room temperature but can transform into gels when heated to body temperature. We first tested whether the chitosan-gel vaccine could release antigen into the NALTs for an extended period of time. We intranasally immunized mice with the chitosan-gel vaccine loaded with OVA conjugated to fluorescein isothiocyanate (FITC-OVA-gel) (*27*) and tracked the persistence of $FITC^+$ cells within the NALTs. As a control, mice were intranasally immunized with the same dose of OVA-FITC resuspended in saline (FITC-OVA). Although the number of $FITC^+$ cells in the NALTs for the first 5 hours after immunization was equivalent across the cohorts, at 24 and 48 hours after immunization, we observed significantly more $FITC^+$ cells in the NALTs recovered from mice that were immunized with the OVA-FITC-gel formulation compared with the control cohort, proving that the gel-based vaccine resulted in sustained antigen release into this structure (Fig. 7D). In addition, the gel-based vaccine also resulted in the recruitment of moDCs into the NALTs (Fig. 7E). We next tested whether the chitosan-gel–based vaccine could evoke T cell activation and proliferation in the NALTs. Because naïve T cells do not readily infiltrate the NALTs (*9*), we assessed the ability of the gel-based vaccine to activate and expand memory $CD8^+$ T cells. Mice with circulating memory OT-I.$CD45.1^+$ $CD8^+$ T cells (generated as described in Materials and Methods) were immunized with either OVA-gel or OVA protein, and 3 days later, animals were injected with 5-bromo-2′-deoxyuridine (BrdU), a synthetic nucleoside analog of thymidine, which is incorporated into the DNA of dividing cells, and the presence of $BrdU^+$ OT-I cells in the NALTs was assessed 1 hour later. In comparison with intranasal delivery of OVA protein, intranasal immunization with OVA-gel resulted in sevenfold more locally dividing ($BrdU^+$) OT-I cells in the NALTs (Fig. 7, F and G). This increased local expansion boosted the total number of OT-I cells in this lymphoid tissue 7.8-fold above that observed after intranasal immunization with OVA protein alone (Fig. 7H). This improvement in local T cell expansion after OVA-gel immunization was dependent on moDCs, as immunization of CCR2 KO memory mice failed to evoke significant local T cell expansion in the NALTs (Fig. 7, I and J). Thus, a sustained vaccine delivery system that results in persistent delivery of antigen into the NALTs and moDC recruitment improves $CD8^+$ T cell activation within this lymphoid tissue.

DISCUSSION

The nasopharyngeal mucosa of the URT is an environment that presents a challenge for the immune system; it is heavily populated with commensal organisms and constantly exposed to environmental antigens, yet it also represents a major entry point into the body for many respiratory pathogens. The immune system must distinguish between the "harmful" and the "harmless" and respond accordingly, mounting robust immune responses to pathogens, yet enforcing tolerogenic responses to commensal organisms and harmless inhaled environmental irritants. Here, we demonstrate that DCs located in the mucosal-associated lymphoid tissue of the URT regulate the balance between immunity and homeostasis to inhaled antigens.

In addition to playing a pivotal role in antigen presentation to drive T cell priming, DCs also have tolerogenic functions, participating in the maintenance of both central and peripheral tolerance (*10*). It is still unclear whether a specific tolerogenic DC lineage exists or whether the suppressor activity of the DC reflects its activation status, with in vivo studies demonstrating that perhaps both can impart tolerogenic properties onto these cells. Hawiger *et al.* (*28*) was first to demonstrate that the induction of self-tolerance or immunity can be controlled by the activation status of DCs. Other studies have identified subsets of DCs with fixed tolerogenic properties that are not altered by maturation. A subset of cDCs expressing perforin (perf-DCs) was shown to limit autoreactive T cells in vivo through a perforin-mediated mechanism (*29*). DCs with tolerogenic properties have been identified in the intestinal mucosa, where they play a central role in enforcing tolerance to commensal bacteria and food antigens (*30*–*32*) as well as the lung (*33*), where they maintain immune quiescence in the airways after inhalation of inert environmental antigens. Recent meta-analysis of the transcriptional landscape during tolerogenic and immunogenic DC maturation revealed that a significant proportion of gene expression changes that occurred during tolerogenic DC maturation overlapped with those changes that occurred during immunogenic DC maturation; this challenges the view that tolerogenic DCs are merely cDCs that have undergone incomplete activation (*34*). With advances in single-cell RNA-seq technology, a clearer picture of the overlapping, yet distinct, maturation trajectories of tolerogenic and immunogenic DCs will likely emerge (*5*).

Here, we provide evidence for another population of cDCs with suppressive properties that reside in the NALTs. Comparing the transcriptional profile of cLN and NALT DC subsets revealed that some of the most differentially expressed genes were mitochondrial genes. Although alterations in expression of these genes has been associated with cell death, changes in mitochondrial gene expression can also be indicative of differences in metabolism. Whether the metabolic state of the NALT DCs is the factor driving high expression of mitochondrial genes will need to be addressed in future studies. Previous reports show that maturation of immunogenic DCs leads to a shift toward a glycolytic metabolic state, whereas, consistent with our data, tolerogenic DCs tend to favor OXPHOS (*12*, *35*). In line with our results, which link the suppressive nature of the NALT DCs to ROS production and changes in DC metabolism, others have previously demonstrated that lung DCs and macrophages induce tolerance to inhaled antigen, and this process was dependent on mitochondrial respiration and peroxisome proliferator-activated receptor gamma (PPARγ)–driven H_2O_2 generation (*33*). Collectively, these reports suggest that the metabolic state of DCs is likely to influence their immunogenicity.

Our results have important implications for the development of vaccines that attempt to evoke cellular immunity after intranasal immunization. The NALTs represent a known site for the deposition of inhaled vaccines (*36*). Here, we show that during the steady state, DCs within the NALTs inhibit T cell responses. However, the suppressive nature of the NALT DC pool is not fixed and can be alleviated by local inflammation that results in the influx of moDCs; these cells dilute out the suppressive DC pool and can facilitate local T cell priming. Collectively, our data highlight two important requirements for an intranasal vaccine that aims to evoke a cellular immune response. The vaccine should, first, trigger the recruitment of moDCs into the NALTs and, second, preserve sufficient amounts of antigen within this region until these immunogenic DCs arrive. Here, we tested a proof-of-concept vaccine and coupled a bio-adhesive polymer and thermosensitive pluronics; this formulation prolonged

antigen retention time in the nasal cavity and evoked moDC recruitment into the NALTs. This vaccine formulation significantly improved T cell priming within the NALTs. Intranasal vaccines need to accommodate for inflammation-induced temporal changes in NALT DC composition and function, if they are to evoke effective T cell immunity. Although the suppressive nature of DCs within the NALTs is an obstacle in the development of intranasal vaccines that aim to evoke strong cellular immunity, it is worth considering that because of the suppressive nature of NALT DCs, intranasal delivery could represent an effective route of administration of treatments that aim to evoke tolerance. Greater understanding of the immunomodulatory effects of the NALT DCs could lead to the development of guided approaches that use these cells for antigen-specific induction of immunosuppression in vivo—this type of DC therapy would be exceptionally beneficial for the treatment of allergic and autoimmune diseases or in transplantation medicine.

Our findings have important implications for the development of intranasally delivered immunotherapies. Better understanding of inflammation-induced temporal changes in NALT DC composition and function will facilitate the development of guided approaches that tip the balance between unresponsiveness and immunity; this could significantly improve the outcomes of intranasal immunotherapies that aim to evoke effective T cell immunity or tolerance.

MATERIALS AND METHODS

Study design

The main aim of the study was to test the antigen presentation capacity of NALT DCs during the steady state and after infection. No outliers were excluded from the data analyses.

Mice and infections

C57BL/6 (CD45.2), B6.CH-2^{bm1} (bm1), OT-I.CD45.1, OT-II.CD45.1, CCR2 KO, and BALB/c mice were bred in-house and housed in specific pathogen–free conditions in the animal facility at the Doherty Institute of Infection and Immunity, the University of Melbourne. All experiments were done in accordance with the Institutional Animal Care and Use Committee guidelines of the University of Melbourne. Mice were infected intranasally in the URT with 10^4 plaque-forming units (PFU) of x31-OVA$_1$ (encodes the OVA$_{257–264}$ epitope within the neuraminidase stalk) (*7*) or 10^4 PFU of x31-OVA$_2$ (encodes the OVA$_{323–339}$ epitope within the neuraminidase stalk) (*8*) in a volume of 10 μl. In some experiments, mice received an URT infection with 10^5 PFU of PR8-LAIV, which was generated as described (*37*). Mice were infected intranasally with 10^8 CFU of *S. aureus* [JKD6159, CA-MRSA (ST93) (*38*)] or *S. aureus* (Newman, MSSA CC8) (*39*) (*40*) in a volume of 10 μl as previously described (*41*).

DC isolation

The NALTs were extracted as described (*9*). cLNs, Peyer's patches, and NALTs recovered from 5 to 10 mice (pooled) were digested with deoxyribonuclease (Roche) and collagenase (Worthington type 3) to generate single-cell suspensions. Light-density cells were selected using Nycodenz (Nycomed Pharma) (1.077 g/cm^3). Spleen and LN DCs were further enriched by depletion of unwanted cells with rat antibodies directed against CD3 (clone KT3-1.1), Thy1 (clone T24/31.7), CD45R (clone RA36B2), Ly6C/G (clone RB6-8C5), Ly-76 (Ter119), and anti-rat Ig magnetic beads (BioMags from Qiagen). All DC subsets were then sort-purified using a BD Aria III (BD Biosciences) into XCR1$^+$ and CD11b$^+$ subsets (gating strategy; fig. S9). Where indicated, DCs were harvested from mice 10 days after the subcutaneous injection of 5×10^6 B16 melanoma cells expressing Flt3 (B16-Flt3-L).

SUPPLEMENTARY MATERIALS

immunology.sciencemag.org/cgi/content/full/5/52/eabb5439/DC1

Supplementary Methods

Fig. S1. Proportion of pDCs in the NALTs.

Fig. S2. NALT DCs suppress T cell proliferation. Related to Fig. 3.

Fig. S3. NALT DCs do not promote T_{reg} formation. Related to Fig. 3.

Fig. S4. NALT DCs suppress T cell proliferation. Related to Fig. 3.

Fig. S5. NALT DCs suppress T cell proliferation and promote T cell death. Related to Fig. 3.

Fig. S6. CD11b$^+$ and XCR1$^+$ NALT DCs express a cDC signature gene profile. Related to Fig. 4.

Fig. S7. NALT DCs express elevated levels of Cox-2 and synthesize PGE_2. Related to Fig. 4.

Fig. S8. moDC recruitment into the NALTs is necessary to alleviate the suppressive nature of the NALT DC pool. Related to Fig. 6.

Fig. S9. Representative fluorescence-activated cell sorting strategy for isolation of NALT DCs.

Table S1. Antibodies used in this investigation.

Table S2. Raw data table.

References (*42*–*52*)

View/request a protocol for this paper from *Bio-protocol*.

REFERENCES AND NOTES

1. I. van der Ven, T. Sminia, The development and structure of mouse nasal-associated lymphoid tissue: An immuno- and enzyme-histochemical study. *Reg. Immunol.* **5**, 69–75 (1993).
2. S. Fukuyama, T. Hiroi, Y. Yokota, P. D. Rennert, M. Yanagita, N. Kinoshita, S. Terawaki, T. Shikina, M. Yamamoto, Y. Kurono, H. Kiyono, Initiation of NALT organogenesis is independent of the IL-7R, LTbetaR, and NIK signaling pathways but requires the Id2 gene and CD3$^-$CD4$^+$CD45$^+$ cells. *Immunity* **17**, 31–40 (2002).
3. T. D. Randall, R. E. Mebius, The development and function of mucosal lymphoid tissues: A balancing act with micro-organisms. *Mucosal Immunol.* **7**, 455–466 (2014).
4. M. Guilliams, C. A. Dutertre, C. L. Scott, N. McGovern, D. Sichien, S. Chakarov, S. van Gassen, J. Chen, M. Poidinger, S. de Prijck, S. J. Tavernier, I. Low, S. E. Irac, C. N. Mattar, H. R. Sumatoh, G. H. L. Low, T. J. K. Chung, D. K. H. Chan, K. K. Tan, T. L. K. Hon, E. Fossum, B. Bogen, M. Choolani, J. K. Y. Chan, A. Larbi, H. Luche, S. Henri, Y. Saeys, E. W. Newell, B. N. Lambrecht, B. Malissen, F. Ginhoux, Unsupervised high-dimensional analysis aligns dendritic cells across tissues and species. *Immunity* **45**, 669–684 (2016).
5. R. Zilionis, C. Engblom, C. Pfirschke, V. Savova, D. Zemmour, H. D. Saatcioglu, I. Krishnan, G. Maroni, C. V. Meyerovitz, C. M. Kerwin, S. Choi, W. G. Richards, A. De Rienzo, D. G. Tenen, R. Bueno, E. Levantini, M. J. Pittet, A. M. Klein, Single-cell transcriptomics of human and mouse lung cancers reveals conserved myeloid populations across individuals and species. *Immunity* **50**, 1317–1334.e10 (2019).
6. H. Lee, D. Ruane, K. Law, Y. Ho, A. Garg, A. Rahman, D. Esterházy, C. Cheong, E. Goljo, A. G. Sikora, D. Mucida, B. K. Chen, S. Govindraj, G. Breton, S. Mehandru, Phenotype and function of nasal dendritic cells. *Mucosal Immunol.* **8**, 1083–1098 (2015).
7. M. R. Jenkins, R. Webby, P. C. Doherty, S. J. Turner, Addition of a prominent epitope affects influenza A virus-specific CD8$^+$ T cell immunodominance hierarchies when antigen is limiting. *J. Immunol.* **177**, 2917–2925 (2006).
8. P. G. Thomas, S. A. Brown, M. Y. Morris, W. Yue, J. So, C. Reynolds, R. J. Webby, P. C. Doherty, Physiological numbers of CD4$^+$ T cells generate weak recall responses following influenza virus challenge. *J. Immunol.* **184**, 1721–1727 (2010).
9. A. Pizzolla, Z. Wang, J. R. Groom, K. Kedzierska, A. G. Brooks, P. C. Reading, L. M. Wakim, Nasal-associated lymphoid tissues (NALTs) support the recall but not priming of influenza virus-specific cytotoxic T cells. *Proc. Natl. Acad. Sci. U.S.A.* **114**, 5225–5230 (2017).
10. M. C. Takenaka, F. J. Quintana, Tolerogenic dendritic cells. *Semin. Immunopathol.* **39**, 113–120 (2017).
11. J. C. Miller, B. D. Brown, T. Shay, E. L. Gautier, V. Jojic, A. Cohain, G. Pandey, M. Leboeuf, K. G. Elpek, J. Helft, D. Hashimoto, A. Chow, J. Price, M. Greter, M. Bogunovic, A. Bellemare-Pelletier, P. S. Frenette, G. J. Randolph, S. J. Turley, M. Merad; Immunological Genome Consortium, Deciphering the transcriptional network of the dendritic cell lineage. *Nat. Immunol.* **13**, 888–899 (2012).
12. F. Malinarich, K. Duan, R. A. Hamid, A. Bijin, W. X. Lin, M. Poidinger, A. M. Fairhurst, J. E. Connolly, High mitochondrial respiration and glycolytic capacity represent a metabolic phenotype of human tolerogenic dendritic cells. *J. Immunol.* **194**, 5174–5186 (2015).
13. V. Kumar, S. Patel, E. Tcyganov, D. I. Gabrilovich, The nature of myeloid-derived suppressor cells in the tumor microenvironment. *Trends Immunol.* **37**, 208–220 (2016).

14. S. Ostrand-Rosenberg, P. Sinha, Myeloid-derived suppressor cells: Linking inflammation and cancer. *J. Immunol.* **182**, 4499–4506 (2009).
15. D. I. Gabrilovich, S. Ostrand-Rosenberg, V. Bronte, Coordinated regulation of myeloid cells by tumours. *Nat. Rev. Immunol.* **12**, 253–268 (2012).
16. Y. Meirow, J. Kanterman, M. Baniyash, Paving the road to tumor development and spreading: Myeloid-derived suppressor cells are ruling the fate. *Front. Immunol.* **6**, 523 (2015).
17. L. L. Hardy, D. A. Wick, J. R. Webb, Conversion of tyrosine to the inflammation-associated analog 3'-nitrotyrosine at either TCR- or MHC-contact positions can profoundly affect recognition of the MHC class I-restricted epitope of lymphocytic choriomeningitis virus glycoprotein 33 by CD8 T cells. *J. Immunol.* **180**, 5956–5962 (2008).
18. Y. P. Hu, Y.-B. Peng, Y.-F. Zhang, Y. Wang, W.-R. Yu, M. Yao, X.-J. Fu, Reactive oxygen species mediated prostaglandin E_2 contributes to acute response of epithelial injury. *Oxid. Med. Cell. Longev.* **2017**, 4123854 (2017).
19. Y. Onodera, T. Teramura, T. Takehara, K. Shigi, K. Fukuda, Reactive oxygen species induce Cox-2 expression via TAK1 activation in synovial fibroblast cells. *FEBS Open Bio* **5**, 492–501 (2015).
20. S. S. Barbieri, S. Eligini, M. Brambilla, E. Tremoli, S. Colli, Reactive oxygen species mediate cyclooxygenase-2 induction during monocyte to macrophage differentiation: Critical role of NADPH oxidase. *Cardiovasc. Res.* **60**, 187–197 (2003).
21. S. Kiritoshi, T. Nishikawa, K. Sonoda, D. Kukidome, T. Senokuchi, T. Matsuo, T. Matsumura, H. Tokunaga, M. Brownlee, E. Araki, Reactive oxygen species from mitochondria induce cyclooxygenase-2 gene expression in human mesangial cells: Potential role in diabetic nephropathy. *Diabetes* **52**, 2570–2577 (2003).
22. A. M. Lone, K. Taskén, Proinflammatory and immunoregulatory roles of eicosanoids in T cells. *Front. Immunol.* **4**, 130 (2013).
23. C. M. Hallissey, R. S. Heyderman, N. A. Williams, Human tonsil-derived dendritic cells are poor inducers of T cell immunity to mucosally encountered pathogens. *J. Infect. Dis.* **209**, 1847–1856 (2014).
24. M. Plantinga, M. Guilliams, M. Vanheerswynghels, K. Deswarte, F. Branco-Madeira, W. Toussaint, L. Vanhoutte, K. Neyt, N. Killeen, B. Malissen, H. Hammad, B. N. Lambrecht, Conventional and monocyte-derived $CD11b^+$ dendritic cells initiate and maintain T helper 2 cell-mediated immunity to house dust mite allergen. *Immunity* **38**, 322–335 (2013).
25. F. Ahmadi, Z. Oveisi, S. M. Samani, Z. Amoozgar, Chitosan based hydrogels: Characteristics and pharmaceutical applications. *Res. Pharm. Sci.* **10**, 1–16 (2015).
26. I.-K. Han, Y. B. Kim, H. S. Kang, D. Sul, W. W. Jung, H. J. Cho, Y. K. Oh, Thermosensitive and mucoadhesive delivery systems of mucosal vaccines. *Methods* **38**, 106–111 (2006).
27. A. J. Highton, T. Kojarunchitt, A. Girardin, S. Hook, R. A. Kemp, Chitosan hydrogel vaccine generates protective CD8 T cell memory against mouse melanoma. *Immunol. Cell Biol.* **93**, 634–640 (2015).
28. D. Hawiger, K. Inaba, Y. Dorsett, M. Guo, K. Mahnke, M. Rivera, J. V. Ravetch, R. M. Steinman, M. C. Nussenzweig, Dendritic cells induce peripheral T cell unresponsiveness under steady state conditions in vivo. *J. Exp. Med.* **194**, 769–780 (2001).
29. Y. Zlotnikov-Klionsky, B. Nathansohn-Levi, E. Shezen, C. Rosen, S. Kagan, L. Bar-On, S. Jung, E. Shifrut, S. Reich-Zeliger, N. Friedman, R. Aharoni, R. Arnon, O. Yifa, A. Aronovich, Y. Reisner, Perforin-positive dendritic cells exhibit an immuno-regulatory role in metabolic syndrome and autoimmunity. *Immunity* **43**, 776–787 (2015).
30. O. Annacker, J. L. Coombes, V. Malmstrom, H. H. Uhlig, T. Bourne, B. Johansson-Lindbom, W. W. Agace, C. M. Parker, F. Powrie, Essential role for CD103 in the T cell-mediated regulation of experimental colitis. *J. Exp. Med.* **202**, 1051–1061 (2005).
31. J. L. Coombes, K. R. R. Siddiqui, C. V. Arancibia-Cárcamo, J. Hall, C. M. Sun, Y. Belkaid, F. Powrie, A functionally specialized population of mucosal $CD103^+$ DCs induces $Foxp3^+$ regulatory T cells via a TGF-β– and retinoic acid–dependent mechanism. *J. Exp. Med.* **204**, 1757–1764 (2007).
32. C. L. Scott, A. M. Aumeunier, A. M. Mowat, Intestinal $CD103^+$ dendritic cells: Master regulators of tolerance? *Trends Immunol.* **32**, 412–419 (2011).
33. A. Khare, M. Raundhal, K. Chakraborty, S. Das, C. Corey, C. K. Kamga, K. Quesnelle, C. St. Croix, S. C. Watkins, C. Morse, T. B. Oriss, R. Huff, R. Hannum, P. Ray, S. Shiva, A. Ray, Mitochondrial H2O2 in lung antigen-presenting cells blocks NF-κB activation to prevent unwarranted immune activation. *Cell Rep.* **15**, 1700–1714 (2016).
34. L. Ardouin, H. Luche, R. Chelbi, S. Carpentier, A. Shawket, F. Montanana Sanchis, C. Santa Maria, P. Grenot, Y. Alexandre, C. Grégoire, A. Fries, T. P. Vu Manh, S. Tamoutounour, K. Crozat, E. Tomasello, A. Jorquera, E. Fossum, B. Bogen, H. Azukizawa, M. Bajenoff, S. Henri, M. Dalod, B. Malissen, Broad and largely concordant molecular changes characterize tolerogenic and immunogenic dendritic cell maturation in thymus and periphery. *Immunity* **45**, 305–318 (2016).
35. E. J. Pearce, B. Everts, Dendritic cell metabolism. *Nat. Rev. Immunol.* **15**, 18–29 (2015).
36. J. F. Mann, R. Acevedo, J. D. Campo, O. Perez, V. A. Ferro, Delivery systems: A vaccine strategy for overcoming mucosal tolerance? *Expert Rev. Vaccines* **8**, 103–112 (2009).
37. Z. Wang, L. Kedzierski, S. Nuessing, B. Y. L. Chua, S. M. Quiñones-Parra, V. C. Huber, D. C. Jackson, P. G. Thomas, K. Kedzierska, Establishment of memory $CD8^+$ T cells with live attenuated influenza virus across different vaccination doses. *J. Gen. Virol.* 97 (2016).
38. S. Sahibzada, S. Abraham, G. W. Coombs, S. Pang, M. Hernández-Jover, D. Jordan, J. Heller, Transmission of highly virulent community-associated MRSA ST93 and livestock-associated MRSA ST398 between humans and pigs in Australia. *Sci. Rep.* **7**, 5273 (2017).
39. M. E. Mulcahy, J. A. Geoghegan, I. R. Monk, K. M. O'Keeffe, E. J. Walsh, T. J. Foster, R. M. McLoughlin, Nasal colonisation by *Staphylococcus aureus* depends upon clumping factor B binding to the squamous epithelial cell envelope protein loricrin. *PLOS Pathog.* **8**, e1003092 (2012).
40. K. B. Kiser, J. M. Cantey-Kiser, J. C. Lee, Development and characterization of a *Staphylococcus aureus* nasal colonization model in mice. *Infect. Immun.* **67**, 5001–5006 (1999).
41. C. Ge, I. R. Monk, S. C. Monard, J. G. Bedford, J. Braverman, T. P. Stinear, L. M. Wakim, Neutrophils play an ongoing role in preventing bacterial pneumonia by blocking the dissemination of *Staphylococcus aureus* from the upper to the lower airways. *Immunol. Cell Biol.* **98**, 577–594 (2020).
42. Y. Liao, G. K. Smyth, W. Shi, The Subread aligner: Fast, accurate and scalable read mapping by seed-and-vote. *Nucleic Acids Res.* **41**, e108 (2013).
43. Y. Liao, G. K. Smyth, W. Shi, featureCounts: An efficient general purpose program for assigning sequence reads to genomic features. *Bioinformatics* **30**, 923–930 (2014).
44. M. D. Robinson, D. J. McCarthy, G. K. Smyth, edgeR: A Bioconductor package for differential expression analysis of digital gene expression data. *Bioinformatics* **26**, 139–140 (2010).
45. M. E. Ritchie, B. Phipson, D. Wu, Y. Hu, C. W. Law, W. Shi, G. K. Smyth, *limma* powers differential expression analyses for RNA-sequencing and microarray studies. *Nucleic. Acids Res.* **43**, e47 (2015).
46. M. D. Robinson, A. Oshlack, A scaling normalization method for differential expression analysis of RNA-seq data. *Genome Biol.* **11**, R25 (2010).
47. C. W. Law, Y. Chen, W. Shi, G. K. Smyth, voom: Precision weights unlock linear model analysis tools for RNA-seq read counts. *Genome Biol.* **15**, R29 (2014).
48. B. Phipson, S. Lee, I. J. Majewski, W. S. Alexander, G. K. Smyth, Robust hyperparameter estimation protects against hypervariable genes and improves power to detect differential expression. *Ann. Appl. Stat.* **10**, 946–963 (2016).
49. R. Kolde, pheatmap: Pretty Heatmaps. R package version 1.0.12. (2019); https://CRAN.R-project.org/package=pheatmap.
50. J. A. Villadangos, M.. Cardoso, R. J. Steptoe, D. van Berkel, J. Pooley, F. R. Carbone, K. Shortman, MHC class II expression is regulated in dendritic cells independently of invariant chain degradation. *Immunity* **14**, 739–749 (2001).
51. L. M. Wakim, A. Woodward-Davis, M. J. Bevan, Memory T cells persisting within the brain after local infection show functional adaptations to their tissue of residence. *Proc. Natl. Acad. Sci. U.S.A.* **107**, 17872–17879 (2010).
52. C. Ge, I. R. Monk, A. Pizzolla, N. Wang, J. G. Bedford, T. P. Stinear, G. P. Westall, L. M. Wakim, Bystander activation of pulmonary Trm cells attenuates the severity of bacterial pneumonia by enhancing neutrophil recruitment. *Cell Rep.* **29**, 4236–4244. e3 (2019).

Acknowledgments: We thank T. Gebhardt (University of Melbourne, Australia) for CCR2 KO mice. **Funding:** This work was supported by National Health and Medical Research Council of Australia (L.M.W.), and C.G. was supported by the China Scholarship Council (C.G.). K.K. is supported by the NHMRC Investigator Grant, NHMRC Senior Research Fellowship and the University of Melbourne Dame Kate Campbell Fellowship. D.H.D.G. and W.R.H. are supported by NHMRC Senior Research Fellowships. **Author contributions:** L.M.W. designed the project with input from D.H.D.G. and W.R.H. L.M.W., J.G.B., C.G., M.H., D.H.D.G., and A.L.G. performed experiments and data analysis. T.H.O.N. and K.K. supplied crucial reagents. S.G.T., M.E., T.L., and S.I.M. provided clinical samples. L.M.W. contributed to statistical analysis and writing and editing of the manuscript. **Competing interests:** L.M.W. is named as an inventor on a provisional patent application filed by the University of Melbourne (2020902546) covering the use of chitosan-hydrogel as part of vaccine formulation against influenza virus. **Data and materials availability:** The data for this study have been deposited in NCBI's Gene Expression Omnibus (www-ncbi-nlm-nih-gov.ezp.lib.unimelb.edu.au/geo) and will be accessible through GEO Series accession number GSE155440.

Submitted 2 March 2020
Accepted 17 September 2020
Published 9 October 2020
10.1126/sciimmunol.abb5439

Citation: J. G. Bedford, M. Heinlein, A. L. Garnham, T. H. O. Nguyen, T. Loudovaris, C. Ge, S. I. Mannering, M. Elliott, S. G. Tangye, K. Kedzierska, D. H. D. Gray, W. R. Heath, L. M. Wakim, Unresponsiveness to inhaled antigen is governed by conventional dendritic cells and overridden during infection by monocytes. *Sci. Immunol.* **5**, eabb5439 (2020).

Unresponsiveness to inhaled antigen is governed by conventional dendritic cells and overridden during infection by monocytes

James G. Bedford, Melanie Heinlein, Alexandra L. Garnham, Thi H. O. Nguyen, Tom Loudovaris, Chenghao Ge, Stuart I. Mannering, Michael Elliott, Stuart G. Tangye, Katherine Kedzierska, Daniel H. D. Gray, William R. Heath and Linda M. Wakim

Sci. Immunol. **5**, eabb5439.
DOI: 10.1126/sciimmunol.abb5439

A nose for inflammation

The nasal-associated lymphoid tissues (NALTs) are lymphoid organs in the nasal mucosa that are sites of inhaled antigen deposition. Here, Bedford *et al*. study induction of immunity in NALTs and identify a role for conventional dendritic cells (cDCs) in suppressing T cell responses during the steady state. Similar cDCs are found in human NALTs in adenoids and tonsils and can also inhibit T cell responses and prevent immune activation. Inflammation induced in nasal mucosa by viral infection induces local recruitment of monocyte-derived DCs, which overrides the effects of cDCs and allows for T cell priming. These results provide mechanistic insight into steady state and inflammatory responses in NALTs.